Original Article

Effect of Tanshinone IIA Versus Tanshinone IIA Loaded Nanocarriers on Folic Acid Induced Chronic Toxicity of Renal Convoluted Tubules in Rats

Amira Neanaa[1], Samia Arafa[1], Moushira El Heneidy[1], Asmaa Ashour[2] and Iman Nabil[1]

[1]*Department of Histology and Cell Biology, Faculty of Medicine, Alexandria University*

[2]*Department of Pharmaceutics, Faculty of Pharmacy, Alexandria University*

ABSTRACT

Objective: Chronic kidney disease (CKD) is associated with irreversible changes. Tanshinone IIA (TAN IIA) is a natural product that could be effective for prevention of CKD, however, its low systemic bioavailability hinders its absorption. Nano-based formula can overcome this problem.

Aim: To compare the histological effect of TAN IIA versus Tanshinone IIA loaded on lipid nanocapsules (TAN IIA-LNCs) on folic acid (FA) induced chronic toxicity of renal convoluted tubules in rats.

Material and Methods: 42 male rats were randomized into: group I; subdivided into 4 subgroups that received saline (control), polyethylene glycol, TAN IIA and TAN IIA-LNCs respectively, for three consecutive days, group II; received a single dose of FA, group III and IV; received TAN IIA and TAN IIA-LNCs respectively, immediately before FA injection and for two consecutive days later on, all by intraperitoneal injection. On day 28, animals were sacrificed and blood samples were obtained to measure the levels of blood urea nitrogen (BUN), serum creatinine, malondialdehyde (MDA), superoxide dismutase (SOD), total antioxidant capacity (TAC) and interlukin-6. Kidney tissues were processed for light and electron microscopic examination. Morphometric studies were done to measure the area percentage of collagen and anti-caspase 3 immunoreactivity. All data was statistically analysed.

Results: Administration of FA resulted in obvious degenerative changes affecting the convoluted tubules. The epithelial cells were distorted with vacuolation, dark and extruded nuclei, mitochondrial changes together with cellular infiltration, widening of the interstitium with collagen deposition, significant increase in BUN, creatinine, MDA, interleukin-6, area percentage of collagen and anti-caspase 3 immunoreactivity with significant reduction in SOD and TAC. Partial preservation of the histological structure and the biochemical parameters were noticed in group III. Meanwhile, group IV showed histological and biochemical results similar to the control.

Conclusion: TAN IIA-LNCs preserved the kidney tubules more than TAN IIA from chronic renal toxicity.

Received: 30 January 2024, **Accepted:** 10 March 2024

Key Words: Convoluted tubules, electron microscope, folic acid, lipid nanocapsules, tanshinone IIA.

Corresponding Author: Amira Neanaa, PhD, Department of Histology and Cell Biology, Faculty of Medicine, Alexandria University, Egypt, **Tel.**: +20 11 1293 3758, **E-mail:** amira.mohamed@alexmed.edu.eg

ISSN: 1110-0559, Vol. 48, No. 1

INTRODUCTION

Chronic kidney disease (CKD) is a clinically prevalent non-infectious disease. It has a progressive pattern and is associated with irreversible changes, thus imposing an enormous burden on public health resources[1]. The management of CKD is targeted on early diagnosis and treatment of the causative agent that contributes to renal fibrosis in order to prevent the disease progression. Additional efforts are exerted to find alternative interventions which could be effective in prevention and also treatment of CKD. The use of natural products derived from natural compounds is considered as a novel strategy for management of patients with CKD[2].

Tanshinones are a class of bioactive compounds present in Salvia miltiorrhiza, which is a popular Chinese herb that has been commonly used in Asian countries especially in China. The primary bioactive constituents among tanshinones are Cryptotanshinone (CPT), Tanshinone I (TAN I) and Tanshinone IIA (TAN IIA), which were reported to have different pharmacological effects including anticancer, anti-inflammatory, cardio and cerebro-vascular protection properties[3].

Among these constituents, TAN IIA gains more attention owing to its lipophilic nature and thus, becomes more pharmacologically active[4]. TAN IIA possesses protective effects on cells and tissues, through controlling the cell proliferation and apoptosis, modulation of the oxidative stress and inflammation as well as inhibition of the fibrosis by decreasing transforming growth factor-β (TGF-β) expression, consequently, attenuation of the structural damage of the cells and tissues occurs[5].

However, TAN IIA was reported to have low systemic bioavailability due to its short half-life and poor aqueous solubility which hinders its clinical utility[6]. Therefore, a

DOI: 10.21608/ejh.2024.266145.2013

nanotechnology-based strategy can be a new promising tool for improving the delivery of TAN IIA to overcome TAN IIA-related problems including diminished oral bioavailability and poor water solubility[7].

The present study was conducted to compare the histological effect of TAN IIA versus Tanshinone IIA loaded nanocapsules (TAN IIA-LNCs) in folic acid induced chronic toxicity of renal convoluted tubules in rats.

MATERIALS AND METHODS

Chemicals

Folic acid (FA) was purchased from Sigma Aldrich (St. Louis, MO, USA). The drug powder was prepared at a dose (250mg/kg) dissolved in 0.5 ml of 0.3 mmol/L sodium bicarbonate (NaHCO3).

Tanshinone IIA (TAN IIA) of purity 98%, was purchased from Baoji Guokang Bio- Technology Co., Ltd China. Preparation of the suspension was done by dissolving TAN IIA in a mixture of polyethylene glycol 400 (PEG 400) with saline at a ratio of 1: 9, respectively.

Tanshinone IIA loaded lipid nanocapsules (TAN IIA-LNCs): Preparation and optimization of TAN IIA-LNCs was carried out at the drug delivery lab at pharmaceutics department, Faculty of Pharmacy, Alexandria University. Preparation of the LNCs was done using the phase inversion method with temperature cycling following the method described previously by Ashour *et al*.[8] For preparation of TAN IIA-LNCs, a specified amount of TAN IIA was dissolved in the oil/surfactant mixture followed by addition of other LNCs ingredients. The same preparation method was adopted as for the blank LNCs. The final concentration of TAN IIA in the LNCs was 0.5 mg/mL[9]. The process of preparation was done in the dark to prevent decomposition of the drug.

Characterization of TAN IIA-LNCs

Colloidal properties

Dilution of the samples with filtered deionized water was done at a ratio of 1:60 v/v[9]. Malvern zetasizer (Nano ZS ,UK) was used for determination of their particle size, poly dispersity index (PDI) and ξ-potential of LNCs.

Determination of TAN IIA entrapment efficiency and drug payload

The entrapment efficiency (EE) was calculated as a percentage using the centrifugation ultrafiltration technique[9]. Dilution of TAN IIA-LNCs with deionized water (1:4, respectively) was done followed by its placement in Vivaspin ® 6 concentrator (MWCO = 100,000, Sartorius, USA). After that, centrifugation was performed at 6000 rpm and 4 °C for 30 min. The amount of the free un-entrapped drug present in the filtrate was measured spectrophotometrically at 270 nm and EE % was calculated by using the following equation:

$$EE\ \% = \frac{\text{Total drug amount-unentraped drug amount}}{\text{Total drug amount}} \times 100$$

Concerning the drug payload, it is presented as the ratio between the weight of entrapped TAN IIA (mg) to the total dry weight of the LNCs (g).

Transmission electron microscopy (TEM)

The morphological features of the prepared LNCs were investigated using TEM (JEM-1400, Tokyo, Japan) at Electron Microscopy unit, Faculty of Science, Alexandria University. A drop of diluted LNC dispersion (either blank or TAN IIA loaded) was placed on a copper grid coated with carbon followed by staining by uranyl acetate solution (2% w/v) for 30 seconds and then left to dry[9].

In-*vitro* drug release study

This study was conducted by using dialysis technique at lab of Pharmaceutics department, Faculty of Pharmacy, Alexandria University. Briefly, 1 mL of either TAN IIA-LNCs or TAN IIA suspension (1 mg/ mL) was placed in pre-soaked dialysis bags (Visking® 36/32, 24 mm, MWCO 12,000–14,000, Serva, USA) which was then immersed in 50% v/v ethanolic water. The drug suspension was prepared in ethanol and water at a ratio of 5.6:1 respectively. The study was performed in a thermostatically controlled shaking water bath at 37 ˚C and 100 rpm. One mL sample was collected at different time points during 24h and substituted with fresh medium. TAN IIA concentration was analysed spectrophotometrically at 270 nm. Afterwards, the % cumulative TAN IIA released was calculated[9].

Animals

Forty-two adult male Wister rats, aged 6-8 weeks and weighing 150-200 g were obtained from the animal house of Physiology department, Faculty of Medicine, Alexandria University. Temperature, humidity and 12 hours light/dark cycle were maintained at standard levels for the laboratory animals. The rats were fed on conventional rat food with water ad libitum for the whole duration of the study. The experimental procedures followed the code of research ethics and approved by the Research Ethics Committee, Alexandria Faculty of Medicine (IRB NO: 00012098-FWA NO: 00018699-approval number: 0201691).

The rats were randomized into four groups

Group I: 24 rats were subdivided into 4 subgroups (n=6), each rat was administered the corresponding daily dose for 3 consecutive days:

- Subgroup IA (Control): received 2.5 mg/kg body weight saline[8].
- Subgroup IB (PEG): received 2.5 mg/kg PEG[8].
- Subgroup IC (TAN IIA): received TAN IIA suspension in a dose of 2.5 mg/kg[8].
- Subgroup ID (TAN IIA-LNCs): received TAN IIA-LNCs in a dose of 2.5 mg/kg[8].

Group II (FA, n=6): each rat received a single dose of 250 mg/kg FA dissolved in 0.5 ml of 0.3 mmol/L NaHCO3[10].

Group III (FA +TAN IIA, n=6): each rat was treated with a daily dose of 2.5 mg/kg of TAN IIA suspension[8] immediately before the FA injection (as in group II)) and on two other consecutive days[10].

Group IV (FA +TAN IIA-LNCs, n=6): each rat treated with a daily dose of 2.5 mg/kg of TAN IIA-LNCs[8] immediately before the FA injection (as in group II) and on two other consecutive days[10].

All the doses were administered by intraperitoneal injection. On the 28th day of the experiment, animals were euthanized under anaesthesia by intraperitoneal injection of 200 mg/kg pentobarbital[11]. Blood samples were collected from abdominal aorta, left for 30 min to clot then centrifuged at 5000 x g for 10 min to isolate the sera and stored at −20 °C for biochemical tests. Both kidneys of all animals were obtained and processed for the histological and immunohistochemical studies as well as for morphometric analysis.

Biochemical tests

Serum blood urea nitrogen (BUN) and serum creatinine level

BUN (mg/dl) was measured according to the manufacturers' manual using enzymatic colorimetric method. Serum creatinine (mg/dl) was estimated according to the manufacturer's protocol using kinetic reaction method.

Malondialdehyde (MDA)

MDA was measured from serum samples according to manufacturers' instructions to assess the oxidative serum levels using colorimetric method. The result was expressed in nmol/ml.

Superoxide dismutase (SOD) and total antioxidant capacity (TAC)

Serum SOD and TAC were measured according to manufacturers' instructions to assess antioxidative serum levels using colorimetric method. The results were expressed in U/ml and mM/L respectively.

Interleukin 6

Serum interleukin 6 (IL-6) was measured as an inflammatory marker according to the manufacturer's protocol based on sandwich enzyme-linked immune-sorbent assay (ELISA) technology. The absorbance was measured at 450 nm. The result was expressed in pg/ml.

Histological studies

A-Light microscopic examination: The right kidneys were fixed in 10% formol saline to be processed by standard procedure to obtain 5µ thick-paraffin sections, stained with hematoxylin and eosin (H&E) and Masson's trichrome respectively[12].

To evaluate the apoptosis, immunohistochemical staining was done. The 5µ thick-paraffin sections (after antigens recovery), were deparaffinized and then 3% H_2O_2 in methanol was added for 10 minutes in order to inactivate any endogenous peroxidase. The sections were firstly incubated in blocking buffer (5% bovine serum albumin in Tris-buffered saline with Tween 20 [TBST]) for 30 minutes then followed by a second incubation overnight with the rabbit polyclonal anti-cleaved caspase-3 primary antibodies (c-caspase 3; 1:1000; #9662; Cell Signaling Technology) at 4°C and then a third incubation with a diluted horseradish peroxidase (HRP)-conjugated secondary antibody (Sigma-Aldrich, USA) at 20-25°C[13].

All stained specimens were examined by the light microscope (Olympus BX41) equipped with a digital camera (Olympus DP20). Histomorphometric analysis was performed from photographs obtained from Masson's trichrome stained specimens as well as immunohistochemical stained kidney sections for the measurement of the area percentage covered by collagen fibers in between the renal tubules as well as the area percentage of anti-c-caspase 3 immunoreactivity respectively[14]. NIH Fiji© Image J software program (version 1.51k, Wayne Rasband, National Institutes of Health, USA) was used. All measurements were statistically analysed.

B-Electron microscopic examination: The left kidneys were cut into small pieces (1mm3) and immediately fixed in 3% phosphate buffered glutaraldehyde. The specimens were further processed to obtain ultrathin sections[15,16] which were examined by TEM (JEM-1400, Tokyo, Japan) at Electron Microscopy unit, Faculty of science, Alexandria University.

Statistical analysis

The biochemical and morphometric results were analyzed using IBM SPSS software package version 20.0. ANOVA test was used for normally distributed quantitative variables to compare between more than two groups. Post Hoc test was used for pairwise comparisons. A result was considered significant at $p\ value \leq 0.05$[17].

RESULTS

Characterization of TAN IIA-LNCs

Colloidal properties

The prepared blank LNCs presented good colloidal properties; size 72.2 ± 2.1 nm, PDI 0.073 ± 0.005 and ξ-potential -15.32 ± 0.62 mV. Meanwhile, TAN IIA-LNCs showed colloidal properties of size; 74.5 ± 1.2 nm, PDI; 0.082 ± 0.003 and ξ-potential -14.6 ± 1.7 mV, denoting that TAN IIA-LNCs didn't affect LNCs' colloidal properties (Figures 1A-D).

Determination of entrapment efficiency and TAN IIA payload

The results revealed efficient TAN IIA loading into the prepared LNCs as the calculated EE% of TAN IIA

and payload were 97.1%± 0.3 and 2.58 ± 0.02 mg/g respectively.

Transmission electron microscopic examination

TEM examination revealed that the prepared LNCs (blank or TAN IIA-LNCs) were spherical and homogenous in shape and individually distributed (Figures 1E,F). Furthermore, both blank and TAN IIA-LNCs had similar morphology, verifying the efficient encapsulation of TAN IIA in the oily core of the developed LNCs.

In *vitro* drug release study

TAN IIA suspension displayed a relatively high burst release ~ 35% after 3 h of the release study with nearly complete release of 85% after 24 h. In contrast, a lower percentage cumulative release of only ~ 52.4% released after 24 h was demonstrated in TAN IIA-LNCs, reflecting the sustainment of TAN IIA release. Additionally, TAN IIA loading into LNCs showed a reduction by ~ 50% in burst release (Figure 1G).

Biochemical results

BUN

The mean level of BUN revealed a significant increase in group II (mean 46.93) compared to all other experimental groups. Although the mean level of BUN was significantly reduced in group III (mean 25.80) in comparison with group II, the level was still significantly higher than groups I (means of different subgroups 17.12, 18.30, 17.70 & 18.03 respectively) and IV (mean 18.63). On the other hand, the mean level of BUN in group IV showed insignificant difference comparable to group I. No significant difference in the mean levels of BUN was detected between the different subgroups of group I (Figure 2A).

Serum Creatinine level

Significantly higher serum creatinine level was shown in group II (mean 1.93) in comparison to the other experimental groups. Meanwhile, the mean level in group III (mean 1.08) was significantly higher compared to groups I (means of different subgroups 0.62, 0.65, 0.62 & 0.67 respectively) & IV (mean 0.67). No significant difference was reported between group IV and I. Similarly, insignificant differences in the mean levels of serum creatinine were noticed between the different subgroups of group I (Figure 2B).

Serum MDA

Serum MDA revealed significantly higher level in group II (mean 14.45) than the other experimental groups. Even though the mean value in group III (mean 7.45) was significantly reduced when compared to group II, the level was significantly higher than groups I (means of different subgroups 4.28, 4.13, 4.13 & 4.43 respectively) and IV (mean 4.43). In group IV insignificant decrease was demonstrated in comparison to group I. In comparing the different subgroups of group I, no significant differences were detected (Figure 2C).

Serum SOD

Significantly lower SOD level was shown in group II (mean 1.39) compared to all experimental groups. In spite of the significant increase in the level of SOD in group III (mean 3.08) in comparison to group II, the level in group III was significantly lower than groups I (means of different subgroups 4.88, 4.64, 4.75 & 4.77 respectively) and IV (mean 4.21). No significant differences were detected either between groups I and IV or between the different subgroups of group I (Figure 2D).

Serum TAC

The mean level of TAC showed significant reduction in group II (mean 0.23) compared to all other experimental groups. The serum level of TAC was significantly elevated in group III (mean 0.51) compared to group II, yet, the level was significantly lower than groups I (means of different subgroups 0.85, 0.84, 0.87 & 0.84 respectively) and IV (mean 0.80). On the other hand, group IV showed insignificant difference with group I. In comparing the different subgroups of group I, insignificant differences were detected (Figure 2E).

Interleukin 6 (IL-6)

The serum IL-6 revealed a significant increase in group II (mean 53) compared to all other groups. Nevertheless, the mean level of IL-6 was significantly higher in group III (mean 26.44) when compared to groups I (means of different subgroups 17.19, 17.65, 17.34 & 17.09 respectively) and IV (mean 17.65). In comparing groups I and IV as well as the different subgroups of group I, no significant differences were detected (Figure 2F).

Histological results

Light microscopic results

A-H&E stain

Group I: The cortex of the control kidney of subgroup IA rats revealed normal renal convoluted tubules separated by a narrow interstitium. The proximal convoluted tubules appeared with narrow or occluded lumina and lined by high cuboidal cells having deeply acidophilic cytoplasm with rounded, vesicular and basal nuclei. On the other hand, the distal convoluted tubules appeared with a wider lumina and lined with low cuboidal cells. The cytoplasm of the lining cells was pale acidophilic, containing rounded, vesicular and apical nuclei. The renal cortical tubules of the other subgroups (IB, IC and ID) illustrated the same histological structure as the control (Figures 3A-H).

Group II: Examination of the renal cortex of the FA group revealed widely spread degenerative changes and necrosis affecting the renal convoluted tubules. The lining cells exhibited cellular vacuolation. Some of their nuclei were dark and small while others were extruded in the tubular lumen. Moreover, the lumina of some proximal tubules appeared wide. Furthermore, widening of the interstitial spaces was depicted in some areas. In addition,

variable degrees of cellular infiltration were noticed around the renal tubules as well as surrounding the congested blood vessels (Figures 4A-D).

Group III: Renal cortical sections of the group which received FA+TAN IIA showed moderate preservation of the structural pattern of the renal tubules as some convoluted tubules appeared more or less normal while others still exhibited degenerative foci. Some proximal tubules displayed wide lumina. Dark and small nuclei were depicted in some of the lining cells together with cytoplasmic vacuolation. Extruded nuclei were encountered in few tubules as well as widening of the interstitial spaces in some areas (Figures 5A,B).

Group IV: Examination of the renal cortex of the group FA+TAN IIA-LNCs revealed evident preservation of the normal morphological appearance of the renal cortex as the histological structure of the cortical convoluted tubules appeared nearly normal similar to the control group apart from few proximal tubules with wide lumina (Figures 5C,D).

B- Masson's trichrome stain

The renal cortex of the control group (subgroup IA) revealed normal distribution of thin collagen fibers between the glomerular tuft of capillaries and in the interstitium between the renal tubules. The same finding was observed during examination of the other subgroups (IB, IC and ID). On the other hand, the FA group (group II) showed excessive deposition of collagen fibers mainly in the interstitium. Moderate amount of collagen fibers in between the glomerular tuft of capillaries and in the interstitium was depicted in the FA+TAN IIA (group III). However, the FA+TAN IIA-LNCs (group IV) displayed normal pattern of collagen fibers distribution either between the glomerular tuft of capillaries or in the interstitium of the renal tubules (Figures 6A-G).

C-Immunohistochemical staining

The renal cortex of the different subgroups of group I revealed minimal anti- c-caspase 3 immunoreactivity with negative reactivity in the cytoplasm of renal tubules. However, in group II (FA group), marked cytoplasmic anti- c-caspase 3 immunoreactivity was depicted inside the lining of the convoluted tubules' cells. Administration of FA+TAN IIA in group III resulted in moderate anti-c-caspase 3 immunoreactivity exhibited in the cytoplasm of the renal tubules. On the other hand, minimal anti-c-caspase 3 immunoreactivity was displayed in the cytoplasm of the cortical renal tubules of group IV which received FA+TAN IIA-LNCs (Figures 7A-G).

D-Histo-morphometric results

The area percentage of collagen: The mean area percentage of collagen did not show any significant differences between the different subgroups of group I (means 1.43, 1.38, 1.05 & 1.22 respectively). Alternatively, group II revealed significant increase in the area percent of collagen deposition (mean 52.34) as compared to the other experimental groups. Although the percentage area of collagen significantly decreased in group III (mean 20.49) in comparison to group II, the result was still significantly higher than groups I and IV (mean 4.0). Meanwhile, group IV showed insignificant value compared to group I (Figure 8A).

The area percentage of anti-c-caspase 3 immunoreactivity: Insignificant differences in the area percentage of anti-c-caspase 3 immunoreactivity were noticed between the different subgroups of group I (means 0.21, 0.46, 0.59 & 0.68 respectively). However, significantly higher level was shown in group II (mean 57.16) in comparison with all other groups. In group III (mean 22.90), the level was significantly lower than group II, yet, it was significantly higher than groups I and IV (mean 2.27). On comparing groups IV and I, no significant difference was detected (Figure 8B).

Electron microscopic results

Group I: Examination of the renal cortex of the control group (subgroup IA) revealed well-organized and densely-packed renal convoluted tubules with minimal interstitium in between occupied by interstitial cells. The proximal tubules were lined by high cuboidal cells with their characteristic apical brush border formed of closely-packed long microvilli. The nuclei were rounded, euchromatic and basally located. The cytoplasm showed numerous apical endocytotic vesicles, lysosomes and abundant elongated mitochondria. The lateral plasma membranes displayed intercellular junctions while the basal membrane exhibited infoldings forming compartments occupied by elongated longitudinally oriented mitochondria. On the other hand, the distal convoluted tubules were lined by low cuboidal cells bared few and short microvilli. Their nuclei were rounded and euchromatic, pushed apically by extensive basal membrane infoldings that formed compartments occupied also by longitudinally arranged mitochondria (Figures 9A-F). The ultrastructural features of the convoluted tubules of the other subgroups (subgroups IB, IC and ID) were the same as the subgroup IA (Figures 10,11,12A-F).

Group II: Ultrastructural examination of the renal cortex of FA group displayed marked degenerative changes affecting the renal convoluted tubules with distortion of their normal architecture as well as widening of the interstitium which was occupied by many interstitial cells and dilated peritubular blood capillaries filled with many red blood cells. The proximal convoluted tubules were obviously affected where their lining epithelium displayed variable ultrastructural changes. Most of their lining cells showed interrupted brush border with extrusion of their cytoplasmic components. Additionally, some cells depicted areas of cytoplasmic rarefaction and degenerative vacuolation. The nuclei of the proximal tubule cells were variably affected. Some were irregular, others were shrunken with clumped heterochromatin while some were extruded into the lumen. The mitochondria were irregularly

arranged where some had bizarre shapes. The basal infoldings were lost in some cells while others depicted some remnants. Moreover, distorted lining epithelium was also depicted in the distal convoluted tubules where irregularly arranged mitochondria were detected. Some of the lining cells exhibited irregular nuclei while others were shrunken. Even though the basal infoldings were observed, they were shallow. Furthermore, numerous collagen fibers were deposited in the interstitium between the convoluted tubules (Figures 13A-H).

Group III: Examination of renal cortices of the FA+TAN IIA revealed a combined preservation of the structure of some convoluted tubules while others still revealed ultrastructural changes. Widening of the interstitial spaces was depicted in some areas. Some of the proximal tubular cells were apparently normal, nevertheless, other lining cells showed widely-spaced microvilli. Nuclei of some cells were rounded, basal and euchromatic although some exhibited peripheral margination of the nucleolus. The cytoplasm showed rarefaction and few basal vacuoles. The mitochondria were irregularly arranged with loss of the basal infoldings in some cells. However, most of the distal tubules appeared normal apart from few lining cells displayed blunted microvillous border, irregularly oriented mitochondria and inconspicuous basal infoldings (Figures 14A-F).

Group IV: Electron micrographs of renal cortex of the FA+TAN IIA-LNCs showed apparently normal architecture of the renal convoluted tubules with almost normal ultrastructural appearance of their lining epithelium inspite of persistence of some degenerative foci. The convoluted tubules appeared tightly-packed with minimal interstitium in between. The majority of the lining cells of the proximal tubules appeared normal, nonetheless few showed slightly irregular nuclei. Meanwhile, the distal convoluted tubules displayed normal appearance similar to the control one (Figures 15A-F).

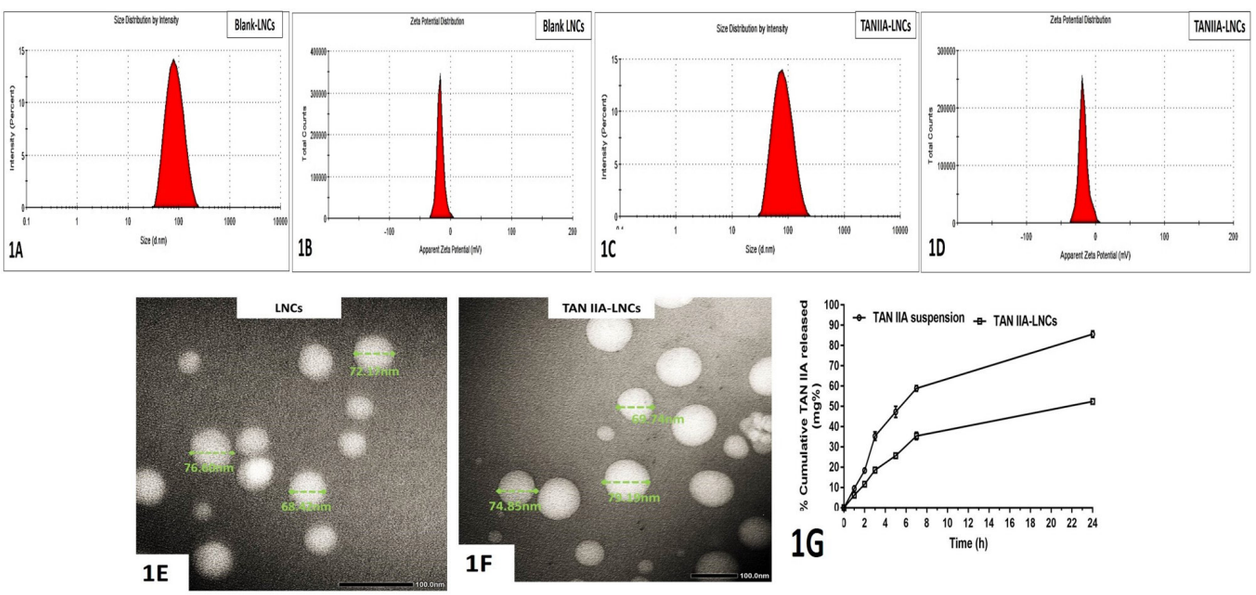

Fig. 1A-G: Characterization of blank LNCs and TANIIA-LNCs: A&B) Size distribution by intensity and zeta potential distribution respectively of blank LNCs. C&D) Size distribution by intensity and zeta potential distribution respectively of TAN IIA-LNCs. E&F) Morphological chracterization by TEM with measurment for blank LNCs and TAN IIA-LNCs respectively. Mic.Mag. x 50.000. G) Percentage cumulative TAN IIA released from TAN IIA suspension and TAN IIA-LNCs.

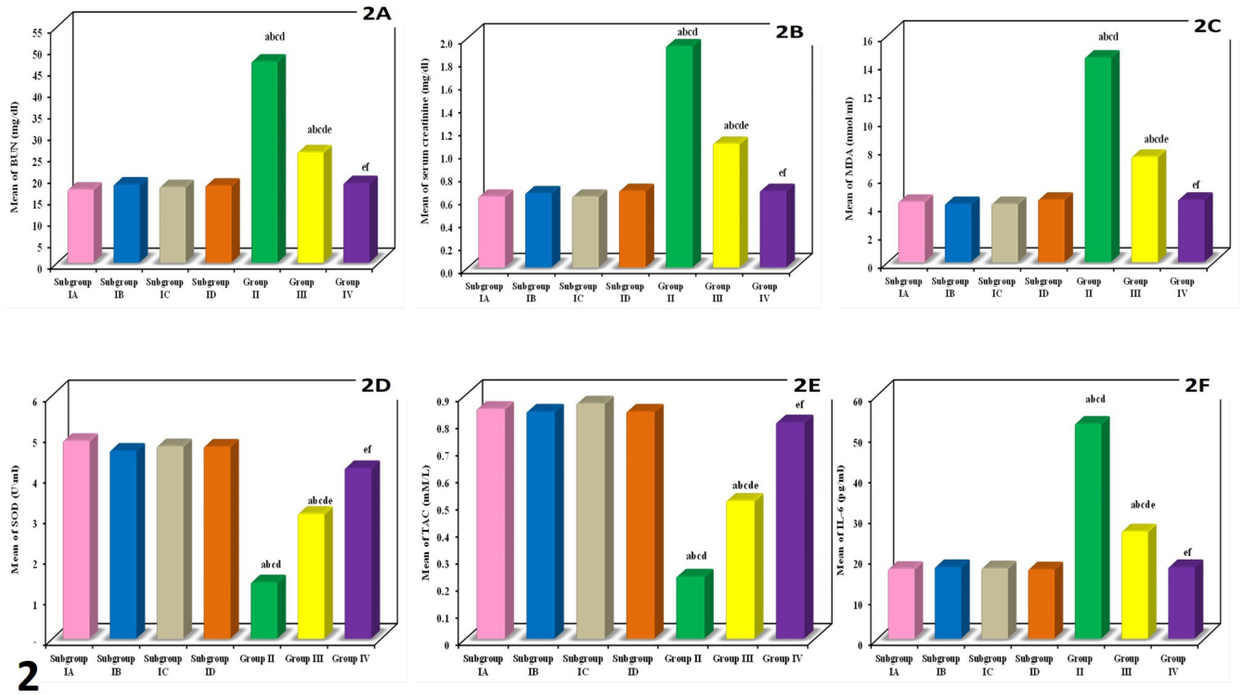

Fig. 2A-F: Bar charts show the mean levels of the different experimental groups. A) BUN in mg/dl, B) Serum creatinin in mg/dl, C) MDA in nmol/ml, D) SOD in U/ml, E) TAC in mM/L and F)IL-6 in pg/ml. Statistically significant at $p \leq 0.05$, a: significant with subgroup IA, b: significant with subgroup IB, c: significant with subgroup IC, d: significant with subgroup ID, e: significant with group II, f: significant with group III.

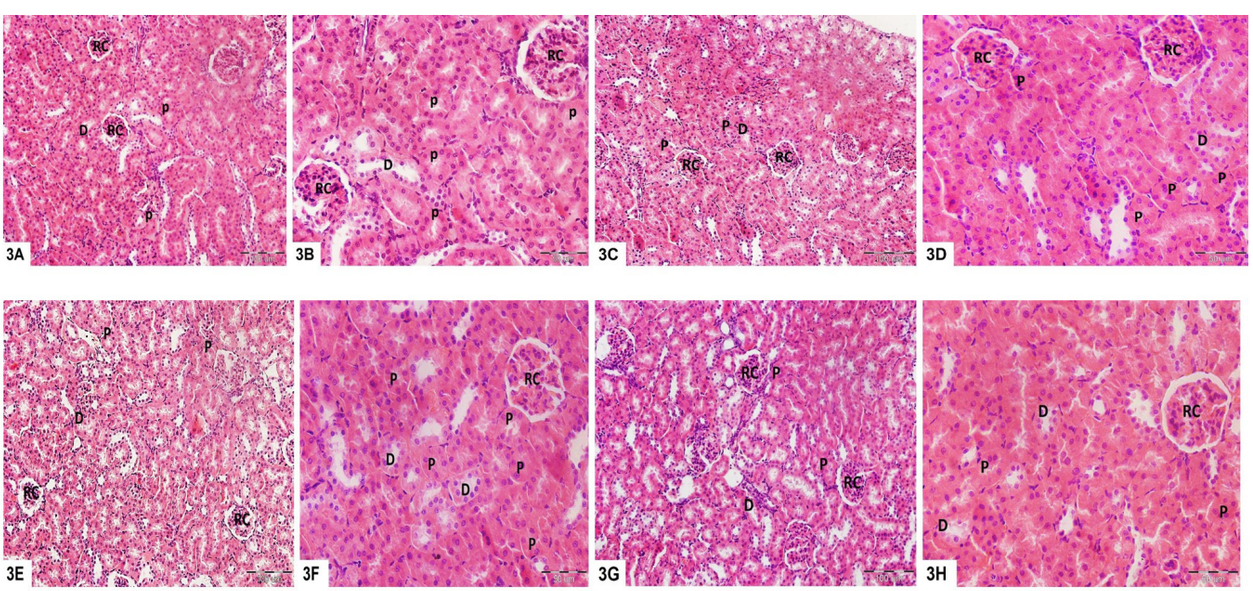

Fig. 3A-H: Photomicrographs of the renal cortex of the different subgroups of group I; A&B:subgroup IA (control), C&D: subgroup IB (PEG), E&F: subgroup IC (TAN IIA) and G&H: subgroup ID (TAN IIA-LNCs) showing normal structure and architecure of renal corpusles (RC), proximal (P) and distal (D) tubules. The proximal tubules (P) appear with a narrow or occluded lumen and lined by high cuboidal cells with deep acidophilic cytoplasm and rounded basal nuclei. The distal tubules display a wider lumen. They are lined by low cuboidal cells with paler acidophilic cytopasm and rounded apical nuclei. H&E stain, Mic. Mag. A,C,E,G x200, B,D,F,H x400

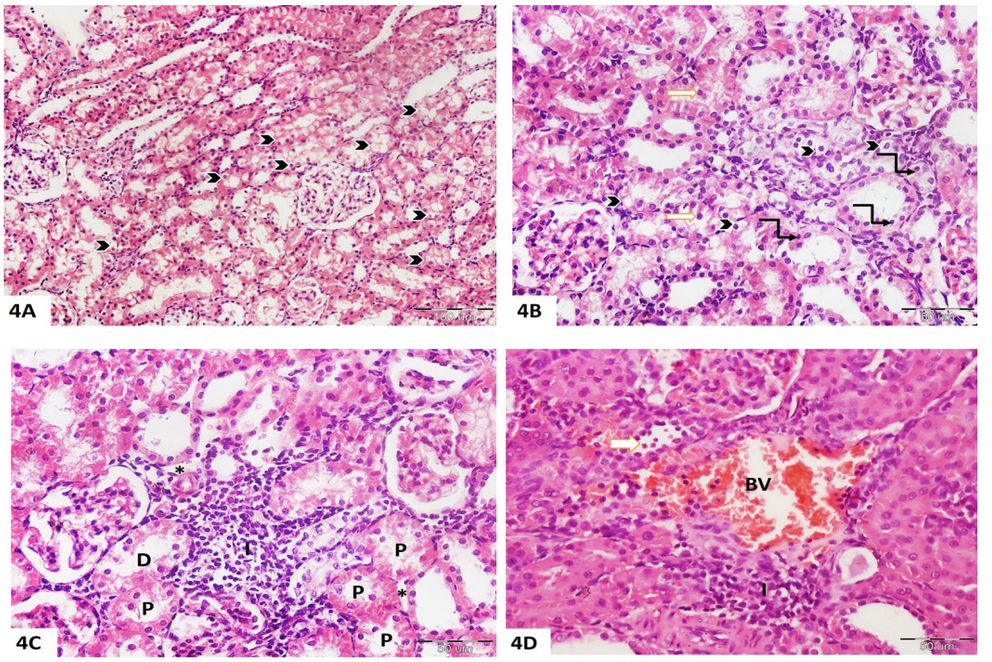

Fig. 4A-D: Photomicrographs of the renal cortex of group II (FA group). A) Marked vacuolation of the lining cells of many convoluted tubules (arrow head). B) Some nuclei of the lining epithelium of the renal tubules appear dark and small (elbow arrow) while others are extruded into the tubular lumen (white arrow). Arrow head; cytoplasmic vacuolation. C) Wide area of cellular infiltration (I) in between the renal tubules with widening of the interstitial spaces (*). P; disrupted proximal tubule cells with wide lumina and D; distal tubules with cytoplasmic vacuolation and lysis. D) A congested blood vessel (BV) in between the cortical renal tubules surrounded by moderate cellular infiltration (I) and desquamated nuclei within a tubular lumen (white arrow). H&E stain, Mic.Mag. Ax200, B-Dx400

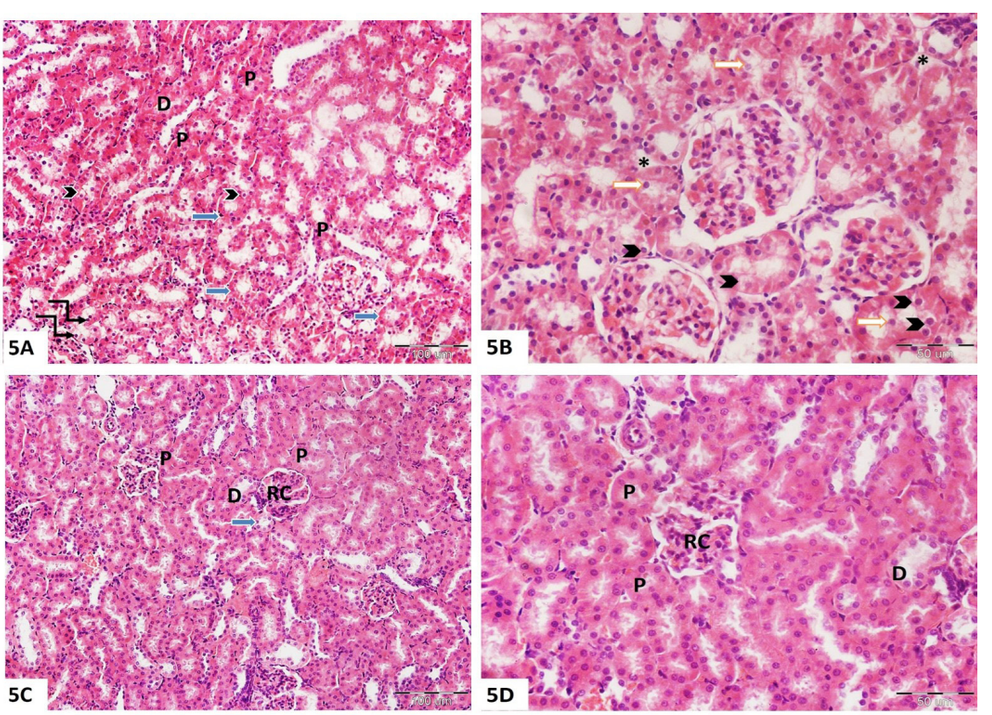

Fig. 5A&B: Photomicrographs of the renal cortex of group III (FA+TAN IIA group). A) Some apparently normal convoluted proximal (P) and distal (D) tubules. Many proximal tubules exhibit wide lumina (blue arrow). Cellular vacuolation (arrow head) and small dark nuclei (elbow arrow) are shown. B) Few tubules display extruded nuclei within their lumina (white arrow) together with widening of the interstitial spaces (*). Arrow head; vacuolated cells. H&E stain, Mic.Mag.Ax200, Bx400 **Fig. 5C&D:** Photomicrographs of the renal cortex of group IV (FA+TAN IIA-LNCs) reveal apparently normal appearance of the proximal (P) and distal (D) tubules. A proximal tubule depicts a wide lumen (blue arrow) in C. RC; renal corpuscles. H&E stain, Mic.Mag.Cx200, Dx400

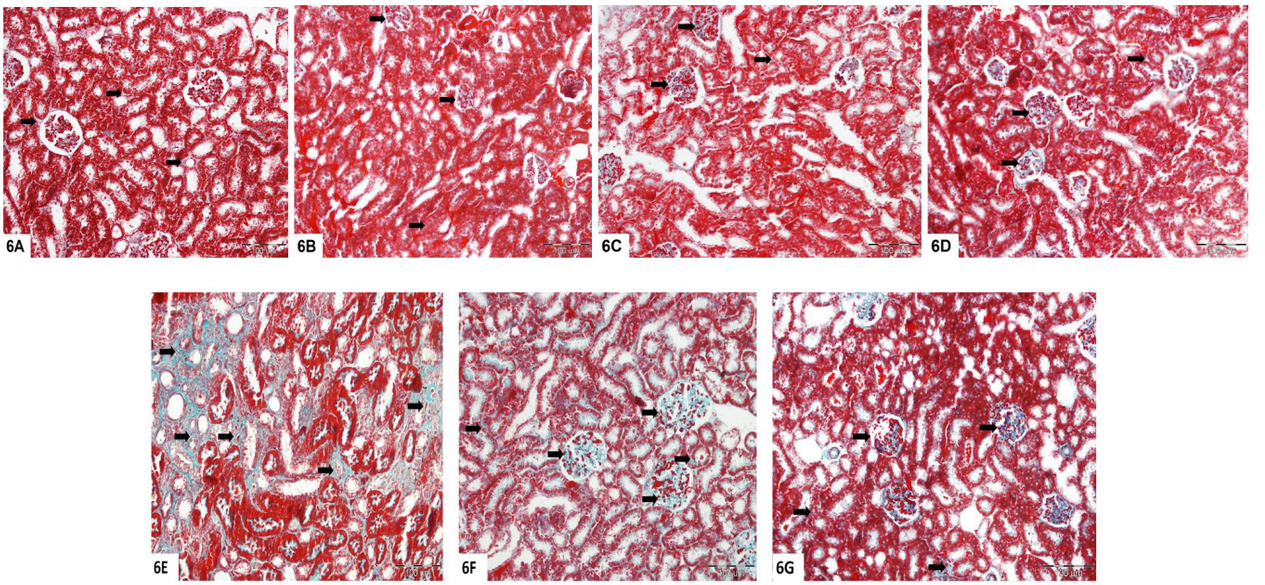

Fig. 6A-G: Photomicrographs of the renal cortex. A-D: group I; A:subgroup IA (control), B: subgroup IB (PEG), C: subgroup IC (TAN IIA) and D: subgroup ID (TAN IIA-LNCs) revealing normal distribution of tiny collagen fibers (arrow) between the glomerular tuft of capillaries and in the interstitium between the renal tubules. E: group II (FA) showing excessive amount of collagen fiber deposition (arrow) mainly in the interstitium between the renal tubules. F: group III (FA+TAN IIA) depicting deposition of moderate amount of collagen fibers (arrow) in between the glomerular tuft of capillaries and in the interstitium. G: group IV (FA+TAN IIA-LNCs) illustrating apparent normal pattern of collagen fibers deposition between the glomerular tuft of capillaries and in the interstitium between the renal tubules. Masson's trichrome stain, Mic. Mag. x200

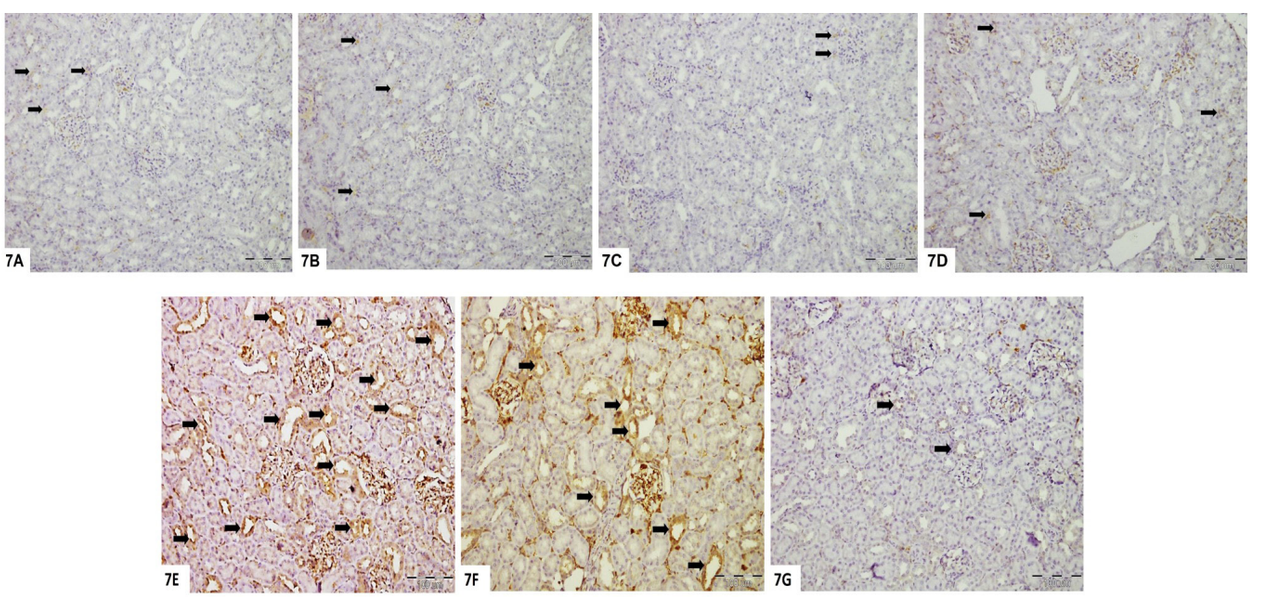

Fig. 7A-G: Photomicrographs of the renal cortex displaying anti-c-caspase 3 immunoreactivity. A-D: group I; A:subgroup IA (control), B: subgroup IB (PEG), C: subgroup IC (TAN IIA) and D: subgroup ID (TAN IIA-LNCs), showing minimal immunoreactivity (black arrows) with negative reactivity in the cytoplasm of the renal convoluted tubules. E: group II (FA) displaying marked cytoplasmic immunoreactivity (black arrows) in the convoluted renal tubule cells. F: group III (FA+TAN IIA) showing moderate immunoreactivity (black arrows) in the cytoplasm of the convoluted tubules. G: group IV minimal immunoreactivity (black arrows)in the cytoplasm of the renal convoluted tubules. Anti- c-caspase 3 IHC, Mic. Mag. x200

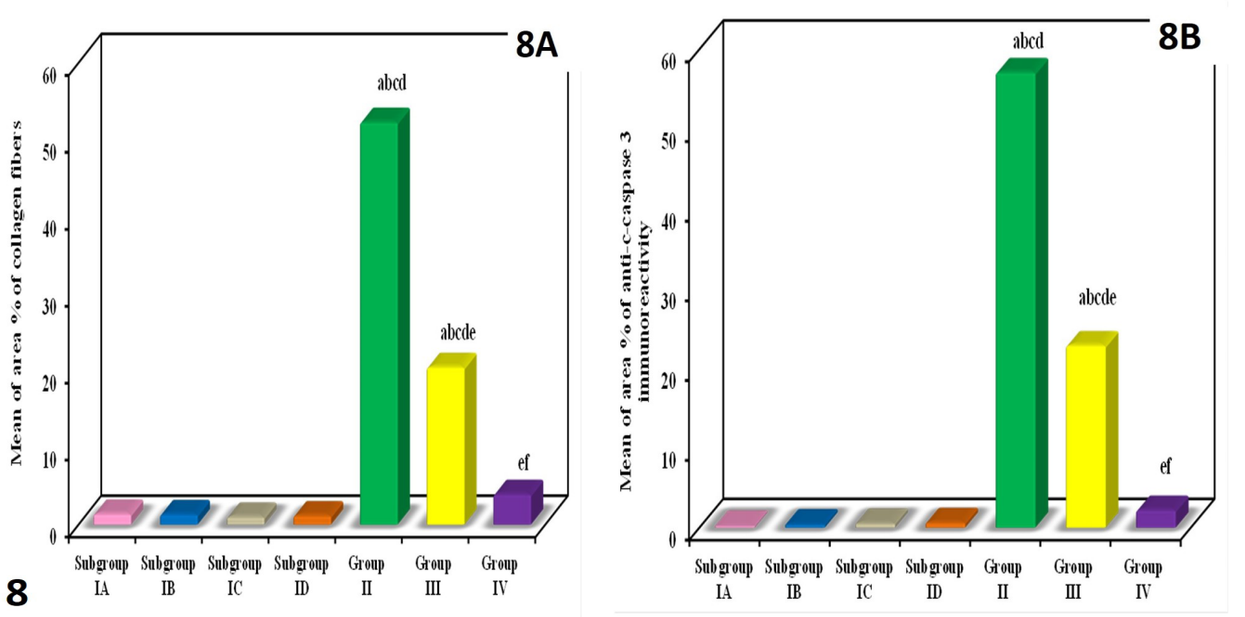

Fig. 8A&B: Bar charts show the mean levels of the different experimental groups. A) Area percentage of collagen fibers and B) Area percentage of anti-caspase3 immunoreactivity. Statistically significant at $p \leq 0.05$, a: significant with subgroup IA, b: significant with subgroup IB, c: significant with subgroup IC, d: significant with subgroup ID, e: significant with group II, f: significant with group III.

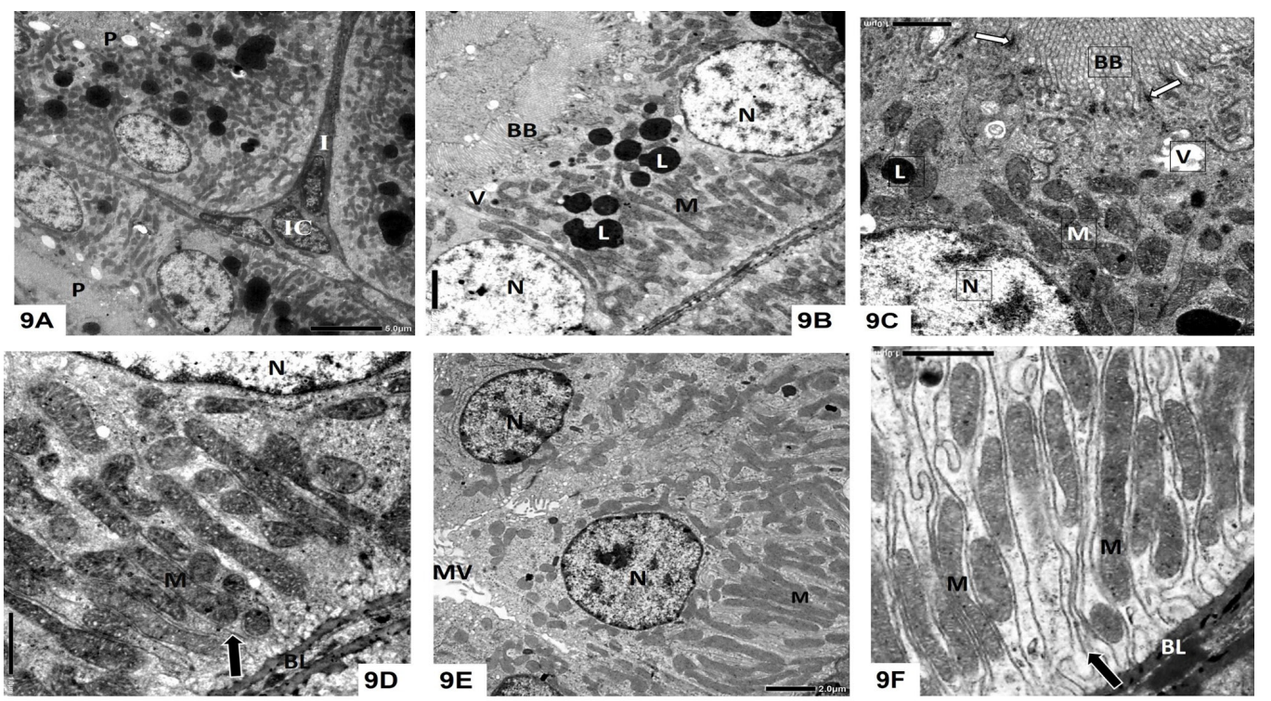

Fig. 9A-F: Electron micrographs of a part of a control renal cortex (subgroup IA). A) Well-organized, densely-packed convoluted tubules with minimal interstitium (I) in between containing interstitial cells (IC). P; proximal tubules. B-D; a proximal tubule: B) The lining cells are high cuboidal with numerous closely packed microvilli forming prominent brush border (BB). The cytoplasm contains a rounded, euchromatic and basal nucleus (N), apical endocytotic vacuoles (V), lysosomes (L) and numerous mitochondria (M). C) A lateral intercellular junction (white arrow) between the lining cells. BB; brush border, N; nucleus, M; mitochondria, V: apical vacuole and L; lysosome. D) A basal part with basal membrane infoldings (black arrow) forming compartments occupied by longitudinally oriented mitochondria (M) with lamellar cristae. N; nucleus, BL; basal lamina. E&F; a distal tubule: E) The epithelial cells are low cuboidal with apical short microvilli (MV). The nuclei (N) are rounded, euchromatic and apical. M; mitochondria. F) A basal part shows extensive basal infoldings (arrow) forming compartments occupied by longitudinally oriented mitochondria (M). BL, basal lamina. Uranyl acetate and lead citrate, Mic.Mag. Ax1200, B&Ex2000, Cx5000, Dx6000, Fx8000

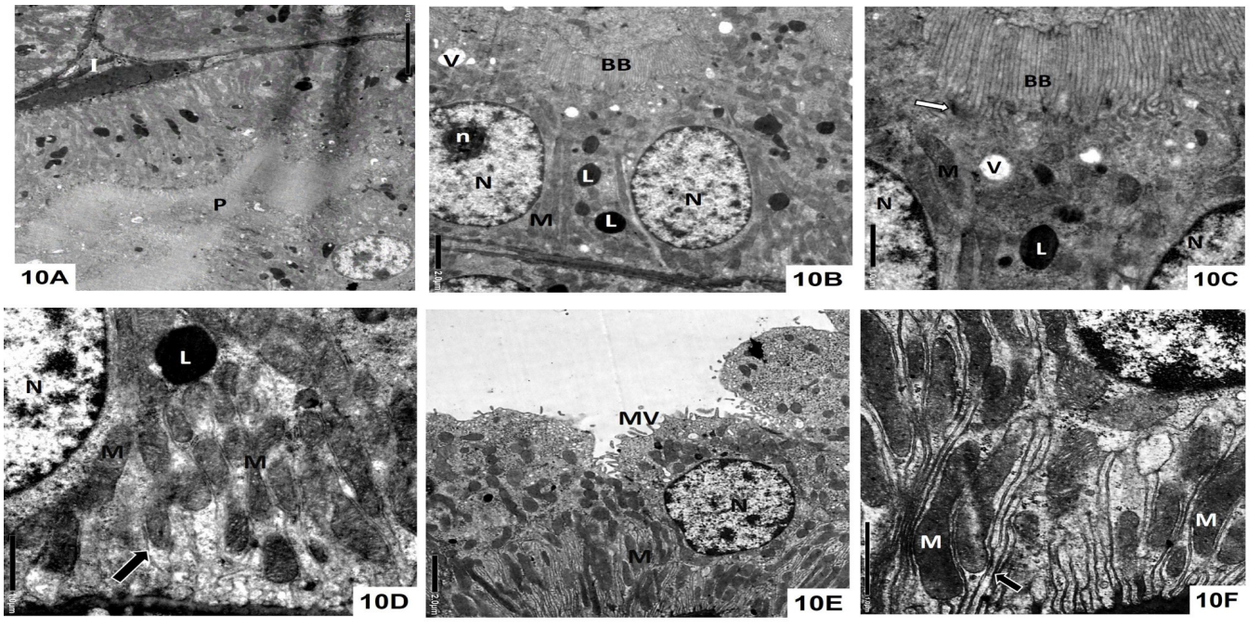

Fig. 10A-F: Electron micrographs of part of renal cortex of subgroup IB (PEG subgroup). A) Closely packed renal tubules separated by a narrow interstitium (I). P; a proximal tubule. B-D; a proximal tubule: B) High cuboidal cells with prominent brush border (BB), euchromatic nuclei (N) with prominent nucleolus (n) and numerous mitochondria (M). L; lysosomes, V; apical endocytotic vacuoles. C) An intercellular junction (white arrow). BB; prominent brush border, V; apical vacuoles, M; mitochondria, N; nucleus and L; lysosome. D) Basal infoldings (black arrow) forming compartments occupied by longitudinally oriented mitochondria (M). N; nucleus, L; lysosome. E&F; a distal tubule: E) Low cuboidal cells with apical short microvilli (MV) and apical euchromatic nucleus (N). F) Complex deep basal infoldings (arrow) occupied by longitudinally oriented mitochondria (M). Uranyl acetate and lead citrate, Mic.Mag. Ax1200, B&Ex2000, Cx5000, Dx6000, Fx8000

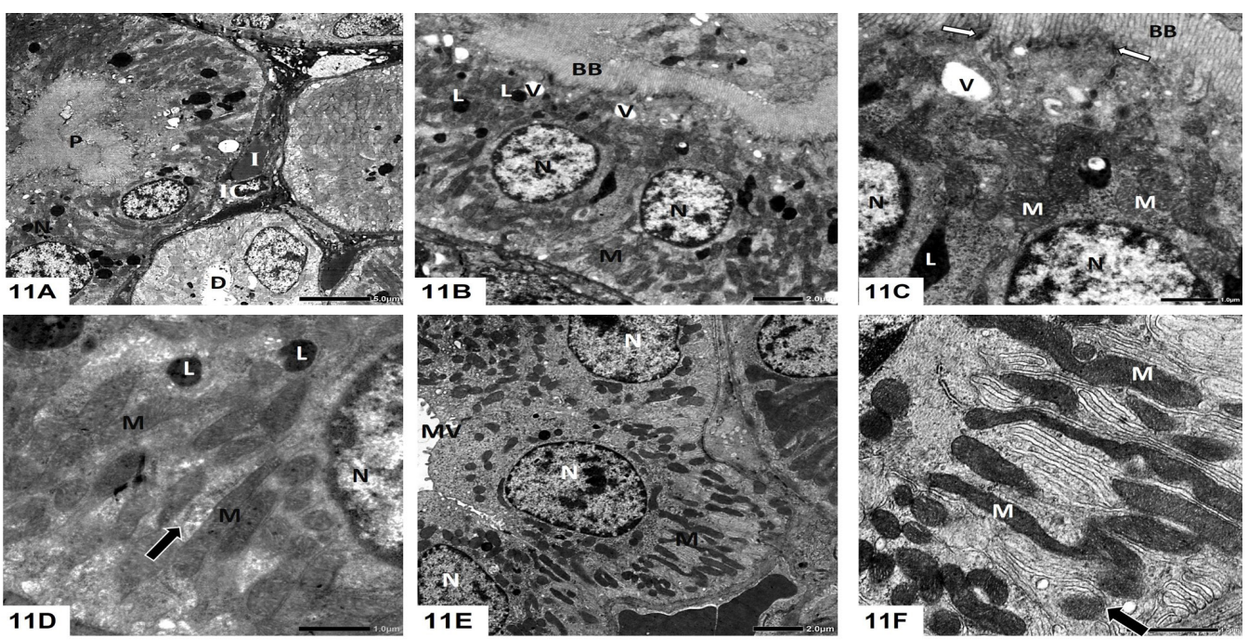

Fig. 11A-F: Electron micrographs of part of renal cortex of subgroup IC (TAN IIA subgroup). A) Cortical tubules with narrow interstitial spaces (I) containing interstitial cells (IC). P; a proximal tubule, D; distal tubule. . B-D; a proximal tubule: B) High cuboidal cells with rounded euchromatic nuclei (N) and an elaborate brush border (BB) narrowing the lumen. M; mitochondria, L; lysosomes and V; apical vacuoles. C) An intercellular junction (white arrow). BB; Brush border, N; nucleus, V; apical vacuoles, M; mitochondria and L; lysosomes. D) Basal compartments formed by the extensive basal infoldings (black arrow) and occupied by elongated mitochondria (M). N; nucleus, L; lysosomes. E&F; a distal tubule E) Low cuboidal cells with apical short microvilli (MV) and apical euchromatic nuclei (N). F) Longitudinally oriented mitochondria (M) occupying compartments formed by extensive basal infoldings (arrow).Uranyl acetate and lead citrate, Mic.Mag. Ax1200, B&Ex2000, Cx5000, Dx6000, Fx8000

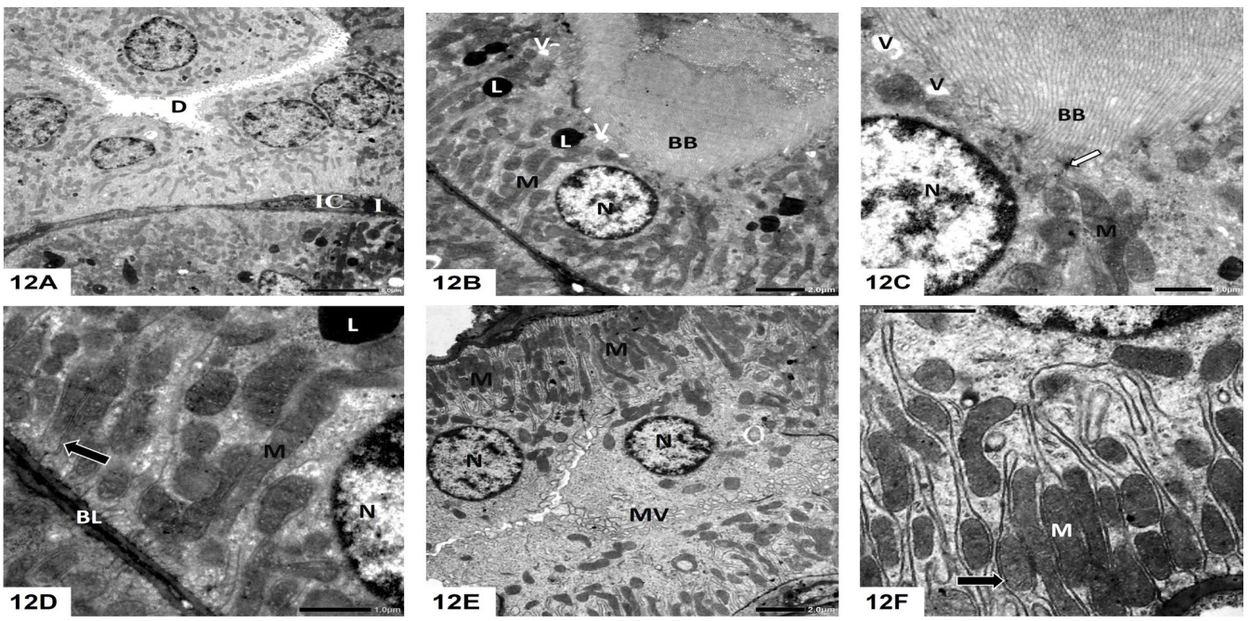

Fig. 12A-F: Electron micrographs of part of renal cortex of subgroup ID (TAN IIA-LNCs subgroup). A) Densely-packed cortical tubules with minimal interstitium (I) containing interstitial cells (IC). D; distal tubule. . B-D; a proximal tubule: B) High cuboidal cells with prominent brush border (BB) obscuring the lumen. N; euchromatic nucleus. M; mitochondria, L; lysosomes and V; apical vacuoles. C) An intercellular junction (white arrow). BB; brush border, N; nucleus, M; mitochondria and V; apical vacuoles. D) Basal infoldings (black arrow), M; longitudinally oriented elongated mitochondria, N; nucleus, L; lysosome and BL; basal lamina. E&F; a distal tubule: E) Low cuboidal cells with apical short microvilli (MV) and apical euchromatic nuclei (N), M; Mitochondria. F) M; Longitudinally oriented mitochondria and arrow; deep basal infoldings. Uranyl acetate and lead citrate, Mic.Mag. Ax1200, B&Ex2000, Cx5000, Dx6000, Fx8000

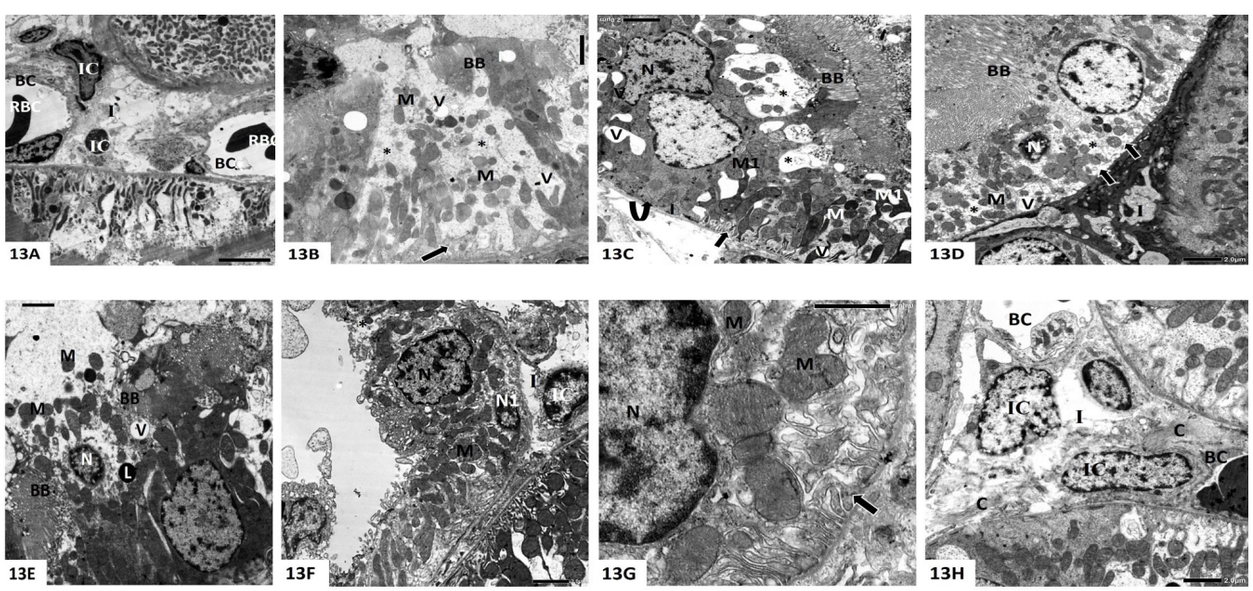

Fig. 13A-H: Electron micrographs of part of renal cortex of group II (FA group). A) Distorted convoluted tubules separated by a wide interstitium (I) occupied by several interstitial cells (IC) and wide peritubular congested blood capillaries (BC) containing red blood corpuscles (RBC). B-E; a proximal tubule: B) Distorted lining cells with disrupted apical plasma membranes. BB; a part of a brush border. Rarified cytoplasm (*) with loss of the regular arrangement of the mitochondria (M). Remnant of basal infoldings are depicted (arrow). V; cytoplasmic vacuoles. C) Lining cells with irregular nuclei (N), rarefied cytoplasm (*) and large vacuoles (V). Irregularly arranged mitochondria (M), some have bizarre shapes (M1). The basal infoldings display remnants in some areas (black arrow) and are lost in another ones (curved up arrow). BB; brush border. D) A shrunken nucleus (N) with clumped heterochromatin, cytoplasmic rarefaction (*) and basal vacuolation (V). M; haphazardly arranged mitochondria with loss of basal infoldings (arrows). BB; brush border and I; widened interstitial space. E) Distorted lining cells with disrupted apical membranes. BB; a part of a brush border. Extrusion of a shrunken heterochromatic nucleus (N) and some organelles. M; mitochondria, V; vacuoles and L; lysosomes. F&G; a distal tubule: F) A lining cell with a shrunken nucleus (N1) with peripheral clumps of the heterochromatin while the neighboring cell has a slightly irregular nucleus (N). M; irregularly arranged mitochondria and I; a wide interstitium with interstitial cells (IC). G) Short irregular basal infoldings (arrow) and bizzare shaped mitochondria (M). N; nucleus. H) Numerous collagen fibers (C) deposited in a wide interstitium (I) occupied by interstitial cells (IC) and peritubular capillaries (BC). Uranyl acetate and lead citrate, Mic.Mag. Ax1200, B-F&Hx2000, Gx8000

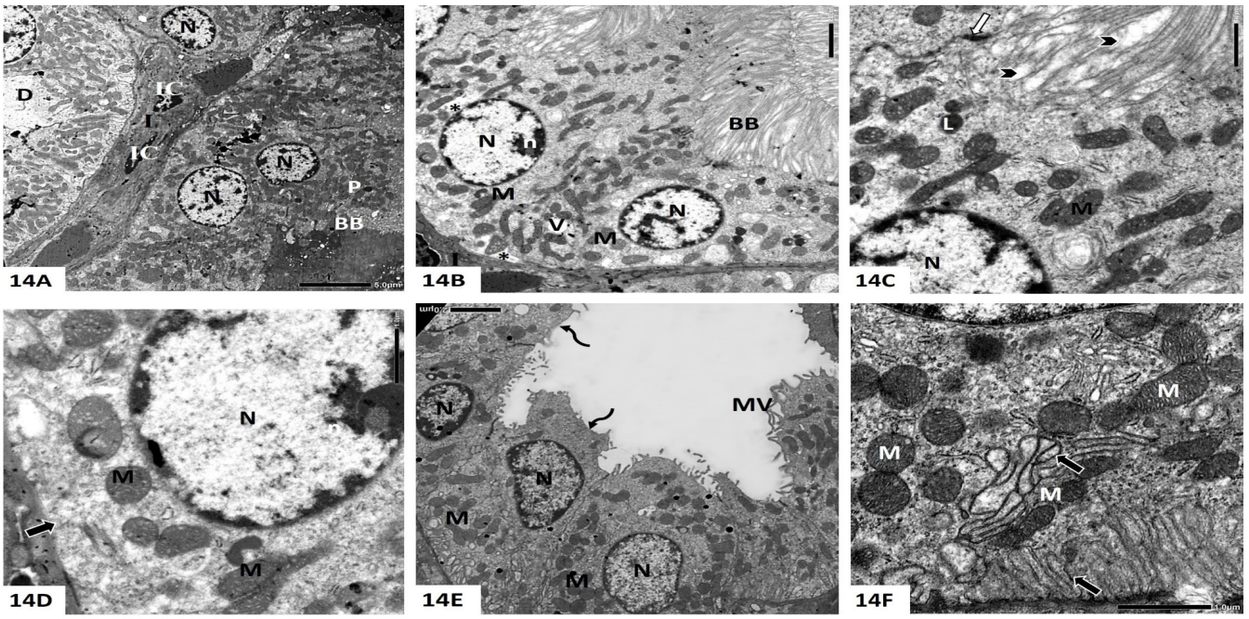

Fig. 14A-F: Electron micrographs of part of renal cortex of group III (FA+TAN IIA group). A) Some convoluted tubules are separated by a wide interstitium (I) which is occupied by interstitial cells (IC). The lining epithelium of the proximal tubules (P) display brush border (BB) and euchromatic nuclei (N). D; distal tubule. B-D; a proximal tubule: B) The nuclei (N) appear rounded, basal and euchromatic with peripheral margination of the nucleolus (n). Areas of rarified cytoplasm (*) with loss of the regular alignment of mitochondria (M). BB; a brush border and I; interstitial space. C) Widely spaced microvilli (arrow head). N; nucleus, M; mitochondria, L; lysosomes and white arrow; intercellular junction. D) Loss of the basal infoldings (arrow). N; nucleus (N) and M; mitochondria. E&F; a distal tubule: E) Lining cells with short and few microvilli (MV) while others show blunted microvillous border (curved arrow). N; rounded and euchromatic nuclei, M; mitochondria. F) Irregularly oriented mitochondria (M) and irregular basal infoldings (black arrow). Uranyl acetate and lead citrate, Mic.Mag. Ax1200, B,C&Ex2000, Dx6000, Fx8000

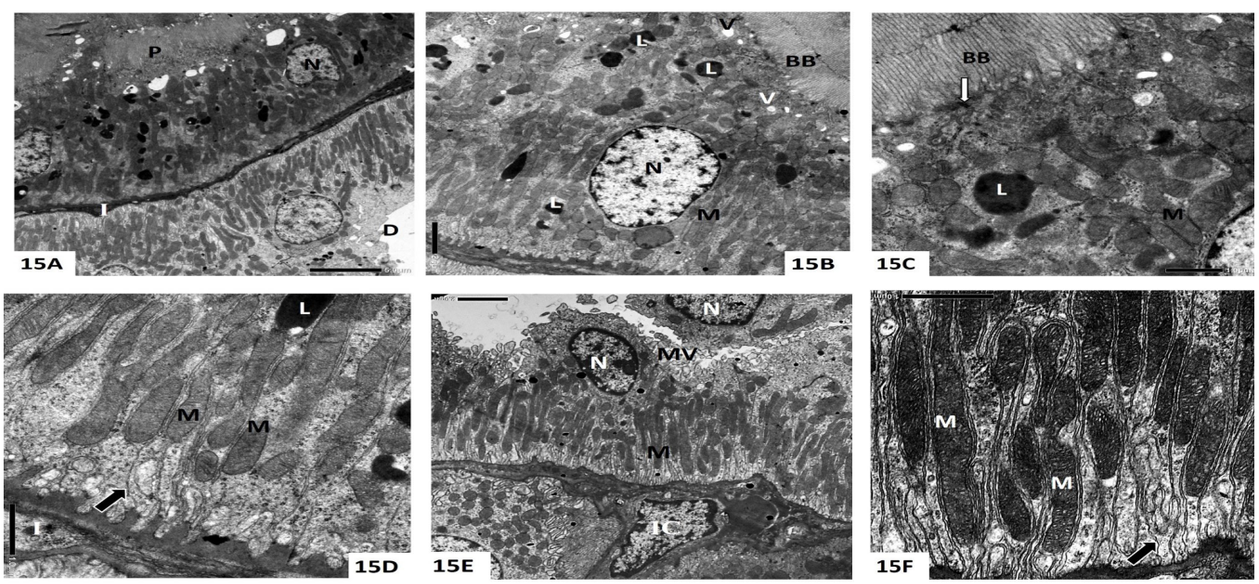

Fig. 15A-F: Electron micrographs of a part of renal cortex of group IV (FA+TAN IIA-LNCs group). A) Nearly normal convoluted tubules with a narrow interstitium (I). N; slightly irregular nuclei within lining cells of a proximal tubule (P). D; a distal tubule. B-D; a proximal tubule: B) A lining cell with prominent brush border (BB), rounded euchromatic and basal nucleus (N), lysosomes (L), apical endocytotic vacuoles (V) and abundant elongated mitochondria (M). C) An intercellular junction (white arrow). BB; brush border, L; lysosome and M; mitochondria. D) Prominent basal infoldings (black arrow) forming compartments occupied by longitudinally oriented mitochondria (M) with lamellar cristae. L; lysosome and I; narrow interstitial space. E&F; a distal tubule: E) Apparently normal lining cells with apical short and few microvilli (MV) and apical euchromatic nuclei (N). IC, interstitial cell. F) Regularly oriented basal infoldings (arrow) forming basal compartments occupied by elongated mitochondria (M). Uranyl acetate and lead citrate, Mic.Mag. Ax1200, B&Ex2000, Cx5000, Dx6000, Fx8000

DISCUSSION

So far, chronic kidney diseases (CKD) are still non curable and once they occur, they have a progressive course which may eventually need either dialysis or kidney transplant[18]. Accordingly, many recent attempts were carried on by using novel compounds derived from natural products in prevention and treatment of CKD[2].

Even though, previous studies have demonstrated that Tanshinone IIA (TAN IIA), exhibited a beneficial reno-protective effect on either AKI or CKD[19-21], its low solubility and oral bioavailability hinder its maximum absorption. Here, nanomedicine emerges as a tool to enhance the therapeutic drugs' benefits and overcome herbal drugs-associated problems[7]. The present work aimed to compare the potential protective effects of TAN IIA versus TAN IIA-loaded nanocapsules (TAN IIA-LNCs) on rat renal convoluted tubules in a folic acid (FA) toxicity model.

Folic acid was used in the current study as an inducer of kidney damage in rats on account of its advantages over the other models[22,23]. FA is a vitamin and hence, it is not toxic. Moreover, it is water soluble and administered by a non-invasive simple intraperitoneal injection, which does not require surgery. Furthermore, FA principally harms the kidney and has no injurious effects on other organs[22,24].

The injection of FA at a high dose (250mg/kg) is commonly used to establish a model for induction of AKI followed by CKD[10,25,26]. The transition from acute to chronic stage is attributed to the low solubility of FA which culminates in crystals' formation within the renal lumen[27]. This leads to a change in cellular architecture and generation of oxidative stress, ultimately fibrosis occur that progress the disease to a chronic form[28]. The selected duration of the whole experiment was 28 days, a period advocated by many previous studies to evaluate the progression of CKD and to assess the renal fibrosis[10,23].

Generally, the investigation of FA toxicity on renal tubule cells relies on assessment of renal function tests and biochemical markers in addition to histological examination of the renal tubules[10,24].

In the current work, the H&E stained kidney sections of the FA group (group II) revealed widespread tubular degenerative changes affecting most of the renal convoluted tubules with distortion of their normal architecture and widened interstitium that depicted massive cellular infiltration as well as capillary congestion. The tubular lining cells showed dark small nuclei, cytoplasmic vacuolation with extrusion of their nuclei reflecting the tubular epithelial cells (TECs) toxicity induced by FA.

The kidney has been established to be the most susceptible organ to folate toxicity due to the high contents of folate receptors,[29] particularly in the cortical TECs which are sensitive to the toxic insults. The proximal tubules (PT) were found to be the most vulnerable region in the nephron to FA-induced damage owing to the existence of ample folate receptors (folate receptor 1) on their luminal sides with high affinity to folate[30,31].

The inflammatory process is a principal nominated mechanism of tubular cell injury. The PT epithelial cells respond to a wide range of insults, with consequential release of bioactive mediators that recruit different inflammatory cells which drive the interstitial inflammation[32]. This mechanism explains the substantial cellular infiltration that was noticed in the current work in the FA group. In addition, the observed peritubular capillary congestion in the FA group could be attributed to the reduction in the vascular resistance of the kidney tissue induced by inflammation that usually accompanies necrosis[33].

In the current work, histomorphometric analysis of the Masson's trichrome stained sections of the FA group revealed significant increase in collagen deposition as compared to the control, confirming the progression to CKD. In consistent with the current results, Jiang *et al*[10] stated that a single dose (250 mg/kg) of FA resulted in substantial collagen deposition in the renal interstitium on day 28, together with increased accumulation of fibronectin. The occurrence of fibrosis is accredited to transforming growth factor β-1 (TGF-β1) production by injured TECs. TGF-β1 is a powerful mitogen for fibroblasts causing their conversion to myofibroblast. Moreover, TGF-β1 induces tubular cell apoptosis as well as epithelial-mesenchymal transition (EMT) program, ultimately, production of an excess extracellular matrix (ECM) occurs[34,35].

The results shown by the light microscopic examination came in line with those of the electron microscope which showed tubular degenerative changes and necrosis affecting most of the renal tubules with disrupted apical membranes and loss of basal infoldings. Some of the tubular cells exhibited shrunken heterochromatic nuclei, vacuolated cytoplasm with extrusion of their cytoplasmic components. The widened interstitium was occupied by several interstitial cells and excess amount of collagen fibers.

It has been suggested that higher concentrations of folic acid induce oxidative stress which acts as the driver of cytotoxicity as an acute effect in kidney epithelial cells and of fibrotic changes as a long term effect. As previously mentioned, the injured TECs produce high levels of TGF-β that elicits EMT of TECs. This process includes disappearance of cell polarity, destruction of tight junctions with damage of renal tubular basement membrane and loss of basal interdigitations. Consequently, the renal TECs enter the interstitium via the injured basement membrane and transform to myofibroblasts[36].

The ultrastructure examination of the FA group revealed irregularly distributed mitochondria which had bizarre shapes. This finding was in agreement with Aparicio-Trejo *et al*[[25] who reported numerous mitochondria with irregular shapes and smaller size in the TECs after 28 days of FA administration. At the subcellular level, mitochondria are specially exposed to high doses of folate and have been

engaged in the progression of these renal diseases into a chronic form. Mitochondria take up almost half of the folate pool resulting in mitochondrial oxidative stress and mitochondrial abnormalities[37]. Additionally, FA elicits the decrease in mitochondrial oxidative phosphorylation capability, and the increase in mitochondrial reactive oxygen species (ROS) triggering the expression of pro-inflammatory cytokines and profibrotic factors, and therefore provoking AKI-to-CKD transition[38]. Persistent disturbance of mitochondrial homeostasis after AKI results in reduction in cellular ATP which causes rapid disturbance of the actin cytoskeleton structure within the apical microvilli, terminal web and junctional complexes and eventually loss of cell polarity occurs[39].

Notably, over production of ROS together with mitochondrial dysfunction increase caspase 3 activities. (10, 24) In the current work, morphometric analysis showed significant high anti- c- caspase 3 immunoreactivity detected in the cytoplasm of most cortical renal tubules of the FA group in comparison to the control subgroup. This finding could elucidate the presence of pyknotic and shrunken heterochromatic nuclei observed by light and electron microscopes respectively.

Also, it has been postulated that the oxidative damage reflected by decreased levels of antioxidant enzymes and enhanced lipid peroxidation, is the culminating event in FA induced kidney disease model[40]. Moreover, as folate accumulates in kidney, it is reduced to tetrahydrofolate by dihydrofolate reductase enzyme which requires large amounts of NADPH. Consequently, all the cellular anti-oxidative systems that consume NADPH become severely impacted[22], resulting in aggravated oxidant/ antioxidant imbalance[41]. In accordance with the present study, significantly high levels of MDA accompanied by significant reduction in SOD and TAC were detected in the FA group compared to the control subgroup.

Inflammation and oxidative stress are closely linked, as they generate a vicious cycle. Different literature have mentioned that a determined inflammatory response provoked by pro-inflammatory cytokines such as IL-6 leading to the persistence of kidney damage[42,43]. In the present study, significant raise of the serum IL-6 was observed in the FA group in comparison to the control subgroup. Similarly, Perales-Quintana *et al*[24] studied the characterization of FA induced kidney disease in rats by analysis of pro-inflammatory cytokines and showed an elevation in IL-6 level in the sera of the FA group in his experiment.

All of the above mentioned histological and biochemical changes in the FA group were essentially reflected upon renal function tests. Serum creatinine and BUN levels have been clinically used as markers of renal functions[44]. Therefore, the current study revealed that the levels of BUN and serum creatinine were significantly higher in the FA group in comparison to the control subgroup denoting sever renal injury and dysfunction induced by high dose of FA.

Many previous literatures clarified the beneficial role of natural products either in prevention or treatment of renal fibrosis[45,46]. TAN IIA was reported to have antioxidant[47], anti-inflammatory[48], anti-fibrotic[49], hepato and neuroprotective effetcs[50,51]. In addition, TAN IIA was found to protect the kidney against diabetic[52] and uric acid nephropathy[53], renal fibrosis[49], renal cell carcinoma[54] and drug induced renal injury[55].

Thus, histological examination of TAN IIA-treated group (group III) showed partial preservation of the structural pattern of the renal tubules. The H&E stained sections revealed some apparently normal renal tubules while others still exhibited degenerative foci in their lining cells in the form of cytoplasmic vacuolation, small dark and extruded nuclei together with mild widening of the interstitial spaces. Moreover, significant reduction in the percentage area of collagen was shown in the TAN IIA treated animals as compared to the FA group.

The results shown by the electron microscopic examination were consistent with those of the light microscope which displayed a combined preservation of the structure of some tubules while others still exhibited fused or widely spaced microvilli, rarified vacuolated cytoplasm and widening of the interstitial spaces. Some irregularly arranged mitochondria were also depicted together with inconspicuous or even lost basal infoldings in some TECs.

Similar histological findings of structural improvement were also encountered by many researchers on studying the effect of TAN IIA on rats with induced kidney injury[56,57]. The renoprotective role of TAN II A is achieved via reduction of the oxidative stress and inflammatory cytokines release, inhibition of cell apoptosis, promotion of autophagy and hindering the direct cellular damage[58]. Moreover, TAN IIA has been demonstrated to possess remarkable antifibrotic properties,[59] particularly, on preventing renal fibrosis[52,60].This is achieved through reduction of ECM deposition and inhibition of EMT through TGF/Smad signaling pathway[61].

Tai *et al*[56] investigated the potential protective effect of TAN IIA in a FA induced kidney injury and concluded that TAN IIA pretreatment was able to lessen the renal damage via decreasing the production of ROS, reducing the expression of inflammatory cytokines, caspase-3 and myeloperoxidase, increasing the expression of pro-survival factor Bcl-2 and improving the mitochondrial function. Hence, in the current work, significant decrease in the anti- c- caspase 3 immunoreactivity was detected in the cytoplasm of the most cortical renal tubules of the TAN IIA group in comparison to the FA one.

The biochemical analysis in the present study further explained the histological results in the TAN IIA-treated group. It showed significant elevation of SOD and TAC levels accompanied by significant reduction of MDA level as compared to the FA group. Numerous studies have delineated that TAN IIA possesses antioxidant properties

and embodies potential to attenuate oxidative stress in *vitro* and in *vivo*[47,62-65]. TAN IIA raises the levels of antioxidant enzymes including SOD, reduced glutathione (GSH) and catalase that scavenge oxygen species and ameliorate oxidative stress preventing the progression of AKI to CKD[62] making TAN IIA a potential antidote for free radical-based disorders[66].

Furthermore, in consistence with the present results, significant reduction in the serum IL-6 level in the TAN IIA group was noticed in comparison to the FA one. Numerous studies have established that TAN IIA reveals fascinating anti-inflammatory effect mediated via lessening of inflammatory mediators specifically interleukin IL-1β, IL-6, and tumour necrosis factor (TNF)-α[64,67]. The present work also showed significant decrease in the kidney function parameters in the TAN IIA group, including BUN and serum creatinine levels comparable to the FA group.

Despite the promising results and the valuable pharmacological properties of TAN IIA, its use is hindered by its physicochemical properties and undesirable pharmacokinetics including the low solubility and poor bioavailability which prevent the complete recovery of the renal injury[58]. Additionally, upon exposure to light and high temperatures (> 80 °C), TAN IIA decomposes with subsequent loss of its biological activity[9]. This suggests that a pre-treatment of TAN IIA could enhance the spontaneous recovery of kidney function and improve the renal salvage process after AKI[57].

Lipid nano capsules (LNCs) are somewhat a novel generation of lipid-based nanovectors, that have been used for drug and gene delivery[68]. Their structure is a mixture between liposomes and polymeric nanocapsules[69]. Moreover, they show a high stability in different biological fluids and are being stable for a long time when prepared by a solvent free and low-energy process[68]. They also offer the capability to encapsulate hydrophilic, lipophilic as well as amphiphilic drugs[70]. They can change both pharmacokinetics and bio-distribution of loaded drugs after parenteral administration[71]. In the present study, the prepared TAN IIA-LNCs possessed good in-*vitro* characteristics as regards colloidal properties, morphology, TAN IIA EE% and TAN IIA release. Furthermore, the in-*vivo* pharmacokinetic study revealed a great enhancement in TAN IIA bioavailability when incorporated into LNCs[9].

The prepared TAN IIA-LNCs improved the bioavailability of TAN IIA by several mechanisms[9]. Among which, the existence of the drug in a molecular solubilized state in the oily cores of LNCs and the avoidance of the possible hepatic first pass metabolism following intraperitoneal administration[72].

Thus, the histological examination of TAN IIA-LNCs treated group (group IV) revealed evident and appreciable preservation of the normal architecture of the kidney tubules. The light microscopic examination using H&E stained sections displayed that the majority of the cortical convoluted tubules were apparently normal and separated by narrow interstitium. Also, the ultrastructure examination came in line with that of the light microscope and showed almost normal appearance of the tubular lining cells apart from some persisting degenerative foci in the form of slightly irregular nuclei.

The observed structural improvement in the cortical renal tubules in TAN IIA-LNCs- treated group indicated that the administration TAN II-LNCs resulted in preservation of the normal renal architecture against FA induced toxicity. This was in consistence with multiple similar studies[73,74].

Sun *et al*[73] used TA IIA loaded into hierarchically structured microcapsules in rats with unilateral obstruction of the ureter. They demonstrated that the bioavailability TAN IIA was considerably improved due to exhibition of superb cellular internalization and transmembrane transport, eventually leading to excellent therapeutic outcomes.

The present study revealed significantly lower percentage area of collagen fibers deposition in Masson's trichrome stained sections in TAN IIA-LNCs-treated group in comparison to the FA and the FA+TAN IIA-treated groups. Ashour *et al*[8] documented that LNCs formulation achieved significantly less collagen fibers deposition when compared to the TAN IIA suspension group in induced liver fibrosis model.

In the current work, significantly lower anti- c- caspase 3 immunoreactivity was detected in the cytoplasm of the majority of cortical renal tubules of TAN IIA-LNCs-treated group in comparison to the FA and the FA+TAN IIA treated ones suggesting the improvement of anti-apoptotic property of TAN IIA. Moreover, the biochemical results showed overall improvement in the antioxidant and renal function parameters and reduction in oxidative stress and inflammatory markers in TAN IIA-LNCs-treated group. The serum level of antioxidant enzymes as SOD and TAC were significantly elevated in TAN IIA-LNCs-treated group in comparison to the FA and the FA+TAN IIA-treated groups. On the other hand, the serum level of MDA and IL-6 in this group revealed significant reduction as compared to the FA and the FA+TAN IIA-treated groups. This was in consistence to the study done by Liu *et al*[75].

All of the previous findings suggested the promising effect of LNCs as a nanocarrier for proper delivery of TAN IIA improving its renoprotective, antioxidant, antiapoptotic, anti-inflammatory and antifibrotic biological activities supporting its use in the prevention of the progression of an acute kidney injury into a chronic state.

CONFLICT OF INTERESTS

There are no conflicts of interest.

REFERENCES

1. Zhou Y, Yang JJCKD. Chronic kidney disease: overview. Chronic Kidney Disease: Diagnosis and Treatment,. 2020:3-12. doi: 10.1007/978-981-32-9131-7_1.
2. Klinkhammer BM, Goldschmeding R, Floege J, Boor PJAickd. Treatment of renal fibrosis—turning challenges into opportunities. Advances in chronic kidney disease. 2017;24(2):117-29. doi: 10.1053/j.ackd.2016.11.002.
3. Cai Y, Zhang W, Chen Z, Shi Z, He C, Chen MJIJoN. Recent insights into the biological activities and drug delivery systems of tanshinones. International Journal of Nanomedicine. 2016;11:121. doi: 10.2147/IJN.S84035.
4. Dai J-P, Zhu D-X, Sheng J-T, Chen X-X, Li W-Z, Wang G-F, *et al*. Inhibition of Tanshinone IIA, salvianolic acid A and salvianolic acid B on Areca nut extract-induced oral submucous fibrosis in *vitro*. Molecules. 2015;20(4):6794-807. doi: 10.3390/molecules20046794.
5. Wang X, Wang W-M, Han H, Zhang Y, Liu J-L, Yu J-Y, *et al*. Tanshinone IIA protected against lipopolysaccharide-induced brain injury through the protective effect of the blood–brain barrier and the suppression of oxidant stress and inflammatory response. Food & Function. 2022;13(15):8304-12. doi: 10.1039/d2fo00710j.
6. Zhai X, Li C, Lenon GB, Xue CC, Li WJajops. Preparation and characterisation of solid dispersions of tanshinone IIA, cryptotanshinone and total tanshinones. asian journal of pharmaceutical sciences. 2017;12(1):85-97. doi: 10.1016/j.ajps.2016.08.004.
7. Qiao L, Han M, Gao S, Shao X, Wang X, Sun L, *et al*. Research progress on nanotechnology for delivery of active ingredients from traditional Chinese medicines. Journal of Materials Chemistry B. 2020;8(30):6333-51. doi: 10.1039/d0tb01260b.
8. Ashour AA, El-Kamel AH, Abdelmonsif DA, Khalifa HM, Ramadan AAJIJoN. Modified lipid nanocapsules for targeted tanshinone IIA delivery in liver fibrosis. International Journal of Nanomedicine. 2021;16:8013. doi: 10.2147/IJN.S331690.
9. Ashour AA, Ramadan AA, Abdelmonsif DA, El-Kamel AHJIJoP. Enhanced oral bioavailability of Tanshinone IIA using lipid nanocapsules: formulation, in-*vitro* appraisal and pharmacokinetics. International Journal of Pharmaceutics. 2020;586:119598. doi: 10.1016/j.ijpharm.2020.119598.
10. Jiang C, Shao Q, Jin B, Gong R, Zhang M, Xu BJBri. Tanshinone IIA attenuates renal fibrosis after acute kidney injury in a mouse model through inhibition of fibrocytes recruitment. BioMed research international. 2015;2015. doi: 10.1155/2015/867140.
11. Laferriere CA, Pang DSJJotAAfLAS. Review of intraperitoneal injection of sodium pentobarbital as a method of euthanasia in laboratory rodents. Journal of the American Association for Laboratory Animal Science. 2020;59(3):254-63. doi: 10.30802/AALAS-JAALAS-19-000081.
12. Suvarna KS, Layton C, Bancroft JD. Bancroft's theory and practice of histological techniques E-Book: Elsevier health sciences; 2018.
13. Bebars SM, Al-Sharaky DR, Gaber MA, Afify DRJJoc, JCDR dr. Immunohistochemical expression of caspase-3 in psoriasis. Journal of clinical and diagnostic research. 2017;11(7):EC01. doi: 10.7860/JCDR/2017/25609.10145.
14. Ferreira T, Rasband WJIF. ImageJ user guide. ImageJ/Fiji. 2012;1:155-61.
15. Glauert AM, Lewis PR. Biological specimen preparation for transmission electron microscopy. Biological Specimen Preparation for Transmission Electron Microscopy: Princeton University Press; 2014.
16. Ellis EAJEMM, Protocols. Staining sectioned biological specimens for transmission electron microscopy: conventional and en bloc stains. Methods and Protocols. 2014:57-72. doi: 10.1007/978-1-62703-776-1_4.
17. Babbie E, Wagner III WE, Zaino J. Adventures in social research: Data analysis using IBM SPSS statistics: Sage Publications; 2022.
18. Eknoyan G, Lameire N, Barsoum R, Eckardt K-U, Levin A, Levin N, *et al*. The burden of kidney disease: improving global outcomes. 2004;66(4):1310-4. doi: 10.1111/j.1523-1755.2004.00894.x.
19. Zhou Z, Qiao Y, Zhao Y, Chen X, Li J, Zhang H, *et al*. Natural products: potential drugs for the treatment of renal fibrosis. 2022;17(1):1-14. doi: 10.1186/s13020-022-00646-z.
20. Zhang W, Liu C, Li J, Lu Y, Li H, Zhuang J, *et al*. Tanshinone IIA: New perspective on the anti-tumor mechanism of A traditional natural medicine. 2022;50(01):209-39. doi: 10.1142/S0192415X22500070.
21. Chen D-Q, Hu H-H, Wang Y-N, Feng Y-L, Cao G, Zhao Y-YJP. Natural products for the prevention and treatment of kidney disease. Phytomedicine. 2018;50:50-60. doi: 10.1016/j.phymed.2018.09.182.
22. Yan LJJAm, medicine e. Folic acid-induced animal model of kidney disease. 2021;4(4):329-42. doi: 10.1002/ame2.12194.

23. Estrela GR, Freitas-Lima LC, Budu A, Arruda ACd, Perilhão MS, Fock RA, *et al*. Chronic kidney disease induced by cisplatin, folic acid and renal ischemia reperfusion induces anemia and promotes GATA-2 activation in mice. Biomedicines. 2021;9(7):769. doi: 10.3390/biomedicines9070769.

24. Perales-Quintana MM, Saucedo AL, Lucio-Gutiérrez JR, Waksman N, Alarcon-Galvan G, Govea-Torres G, *et al*. Metabolomic and biochemical characterization of a new model of the transition of acute kidney injury to chronic kidney disease induced by folic acid. 2019;7:e7113. doi: 10.7717/peerj.7113.

25. Aparicio-Trejo OE, Avila-Rojas SH, Tapia E, Rojas-Morales P, León-Contreras JC, Martínez-Klimova E, *et al*. Chronic impairment of mitochondrial bioenergetics and β-oxidation promotes experimental AKI-to-CKD transition induced by folic acid. Free Radical Biology and Medicine. 2020;154:18-32. doi: 10.1016/j.freeradbiomed.2020.04.016.

26. Jiang C, Zhu W, Yan X, Shao Q, Xu B, Zhang M, *et al*. Rescue therapy with Tanshinone IIA hinders transition of acute kidney injury to chronic kidney disease via targeting GSK3β. Scientific reports. 2016;6(1):1-15. doi: 10.1038/srep36698.

27. Aparicio-Trejo OE, Reyes-Fermín LM, Briones-Herrera A, Tapia E, León-Contreras JC, Hernández-Pando R, *et al*. Protective effects of N-acetyl-cysteine in mitochondria bioenergetics, oxidative stress, dynamics and S-glutathionylation alterations in acute kidney damage induced by folic acid. Free Radical Biology and Medicine,. 2019;130:379-96. doi: 10.1016/j.freeradbiomed.2018.11.005.

28. Krata N, Zagożdżon R, Foroncewicz B, Mucha KJAiete. Oxidative stress in kidney diseases: the cause or the consequence? 2018;66:211-20. doi: 10.1007/s00005-017-0496-0.

29. Nazki FH, Sameer AS, Ganaie BAJG. Folate: metabolism, genes, polymorphisms and the associated diseases. 2014;533(1):11-20. doi: 10.1016/j.gene.2013.09.063.

30. Samodelov SL, Gai Z, Kullak-Ublick GA, Visentin MJN. Renal reabsorption of folates: pharmacological and toxicological snapshots. 2019;11(10):2353. doi: 10.3390/nu11102353.

31. Zhu F, Shin OLCL, Xu H, Zhao Z, Pei G, Hu Z, *et al*. Melatonin promoted renal regeneration in folic acid-induced acute kidney injury via inhibiting nucleocytoplasmic translocation of HMGB1 in tubular epithelial cells. 2017;9(4):1694-707.

32. Liu B-C, Tang T-T, Lv L-L, Lan H-YJKi. Renal tubule injury: a driving force toward chronic kidney disease. 2018;93(3):568-79. doi: 10.1016/j.kint.2017.09.033.

33. Gómez H, Kellum JAJCcn. Sepsis-induced acute kidney injury. Critical care nephrology. 2019:524-33. e3. doi: 10.1016/B978-0-323-44942-7.00090-X.

34. Song S, Qiu D, Luo F, Wei J, Wu M, Wu H, *et al*. Knockdown of NLRP3 alleviates high glucose or TGFB1-induced EMT in human renal tubular cells. 2018;61(3):101-13. doi: 10.1530/JME-18-0069.

35. Yang J, Antin P, Berx G, Blanpain C, Brabletz T, Bronner M, *et al*. Guidelines and definitions for research on epithelial–mesenchymal transition. 2020;21(6):341-52. doi: 10.1038/s41580-020-0237-9.

36. Kandel R, Singh KPJCRiT. Higher concentrations of folic acid cause oxidative stress, acute cytotoxicity, and long-term Fibrogenic changes in kidney epithelial cells. 2022;35(11):2168-79. doi: 10.1021/acs.chemrestox.2c00258.

37. Wijerathne CUB. Regulation of folate reabsorption and oxidative stress in acute kidney injury. 2023. doi: 10.3390/antiox11061046.

38. Fontecha-Barriuso M, Lopez-Diaz AM, Guerrero-Mauvecin J, Miguel V, Ramos AM, Sanchez-Niño MD, *et al*. Tubular mitochondrial dysfunction, oxidative stress, and progression of chronic kidney disease. 2022;11(7):1356. doi: 10.3390/antiox11071356.

39. Devarajan P. Acute Kidney Injury: Pathophysiology, Diagnosis and Prevention. Pediatric Kidney Disease: Springer; 2023. p. 1365-411.

40. Li X, Zou Y, Fu Y-Y, Xing J, Wang K-Y, Wan P-Z, *et al*. Ibudilast attenuates folic acid–induced acute kidney injury by blocking pyroptosis through TLR4-mediated NF-κB and MAPK signaling pathways. 2021;12:650283. doi: 10.3389/fphar.2021.650283.

41. Yan L-JJB. NADH/NAD+ redox imbalance and diabetic kidney disease. 2021;11(5):730. doi: 10.3390/biom11050730.

42. Garbers C, Heink S, Korn T, Rose-John SJNrDd. Interleukin-6: designing specific therapeutics for a complex cytokine. 2018;17(6):395-412. doi: 10.1038/nrd.2018.45.

43. Chen L, Deng H, Cui H, Fang J, Zuo Z, Deng J, *et al*. Inflammatory responses and inflammation-associated diseases in organs. 2018;9(6):7204. doi: 10.18632/oncotarget.23208.

44. Kalantar-Zadeh K, Jafar TH, Nitsch D, Neuen BL, Perkovic VJTl. Chronic kidney disease. 2021;398(10302):786-802. doi: 10.1016/S0140-6736(21)00519-5.

45. Ruiz-Ortega M, Rayego-Mateos S, Lamas S, Ortiz A, Rodrigues-Diez RRJNRN. Targeting the progression of chronic kidney disease. Nature Reviews Nephrology. 2020;16(5):269-88. doi: 10.1038/s41581-019-0248-y.

46. Zhong Y, Deng Y, Chen Y, Chuang PY, He JCJKi. Therapeutic use of traditional Chinese herbal medications for chronic kidney diseases. Kidney international. 2013;84(6):1108-18. doi: 10.1038/ki.2013.276.

47. Wang P, Zhou S, Xu L, Lu Y, Yuan X, Zhang H, *et al*. Hydrogen peroxide-mediated oxidative stress and collagen synthesis in cardiac fibroblasts: blockade by tanshinone IIA. Journal of ethnopharmacology. 2013;145(1):152-61. doi: 10.1016/j.jep.2012.10.044.

48. Li W, Zhang Y, Xing C, Zhang MJIi. Tanshinone IIA represses inflammatory response and reduces radiculopathic pain by inhibiting IRAK-1 and NF-κB/p38/JNK signaling. International immunopharmacology. 2015;28(1):382-9. doi: 10.1016/j.intimp.2015.06.032.

49. Li Y, Deng X, Zhuang W, Li Y, Xue H, Lv X, *et al*. Tanshinone IIA down-regulates-transforming growth factor beta 1 to relieve renal tubular epithelial cell inflammation and pyroptosis caused by high glucose. Bioengineered. 2022;13(5):12224-36. doi: 10.1080/21655979.2022.2074619.

50. Shi M-J, Dong B-S, Yang W-N, Su S-B, Zhang HJB, Pharmacotherapy. Preventive and therapeutic role of Tanshinone IIA in hepatology. Biomedicine & Pharmacotherapy. 2019;112:108676. doi: 10.1016/j.biopha.2019.108676.

51. Jiang Z, Gao W, Huang LJFiP. Tanshinones, critical pharmacological components in Salvia miltiorrhiza. Frontiers in Pharmacology. 2019:202. doi: 10.3389/fphar.2019.00202.

52. Xu S, He L, Ding K, Zhang L, Xu X, Wang S, *et al*. Tanshinone IIA ameliorates streptozotocin-induced diabetic nephropathy, partly by attenuating PERK pathway-induced fibrosis. Drug design, development and therapy. 2020:5773-82. doi: 10.2147/DDDT.S257734.

53. Zhang X-W, Zhou M, An L, Zhang P, Li P, Chen JJTAJoCM. Lipophilic extract and tanshinone IIA derived from salvia miltiorrhiza attenuate uric acid nephropathy through suppressing oxidative stress-activated MAPK pathways. The American Journal of Chinese Medicine. 2020;48(06):1455-73. doi: 10.1142/S0192415X20500718.

54. Kim NY, Jung YY, Yang MH, Chinnathambi A, Govindasamy C, Narula AS, *et al*. Tanshinone IIA exerts autophagic cell death through down-regulation of β-catenin in renal cell carcinoma cells. Biochimie. 2022;200:119-30. doi: 10.1016/j.biochi.2022.05.018.

55. Dou J-Y, Zhang M, Cen H, Chen Y-Q, Wu Y-F, Lu F, *et al*. Salvia miltiorrhiza bunge (Danshen) and bioactive compound tanshinone IIA alleviates cisplatin-induced acute kidney injury through regulating PXR/NF-κB signaling. 2022;13:860383. doi: 10.3389/fphar.2022.860383.

56. Tai H, Cui X-Z, He J, Lan Z-M, Li S-M, Li L-B, *et al*. Renoprotective effect of Tanshinone IIA against kidney injury induced by ischemia-reperfusion in obese rats. Aging (Albany NY). 2022;14(20):8302. doi: 10.18632/aging.204304.

57. Jiang C, Zhu W, Shao Q, Yan X, Jin B, Zhang M, *et al*. Tanshinone IIA protects against folic acid-induced acute kidney injury. The American Journal of Chinese Medicine. 2016;44(04):737-53. doi: 10.1142/S0192415X16500403.

58. Chen Z, Feng H, Peng C, Zhang Z, Yuan Q, Gao H, *et al*. Renoprotective Effects of Tanshinone IIA: A Literature Review. Molecules. 2023;28(4):1990. doi: 10.3390/molecules28041990.

59. Bi Z, Wang Y, Zhang WJB, Pharmacotherapy. A comprehensive review of tanshinone IIA and its derivatives in fibrosis treatment. Biomedicine & Pharmacotherapy. 2021;137:111404. doi: 10.1016/j.biopha.2021.111404.

60. Gao J, Yang G, Pi R, Li R, Wang P, Zhang H, *et al*. Tanshinone IIA protects neonatal rat cardiomyocytes from adriamycin-induced apoptosis. Translational Research. 2008;151(2):79-87. doi: 10.1016/j.trsl.2007.11.005.

61. Cao L, Huang B, Fu X, Yang J, Lin Y, Lin FJMMR. Effects of tanshinone IIA on the regulation of renal proximal tubular fibrosis. Molecular Medicine Reports. 2017;15(6):4247-52. doi: 10.3892/mmr.2017.6498.

62. Yang G, Jia L, Wu J, Ma Y, Cao H, Song N, *et al*. Effect of tanshinone IIA on oxidative stress and apoptosis in a rat model of fatty liver. 2017;14(5):4639-46. doi: 10.3892/etm.2017.5162.

63. Chen W, Chen GJCPD. Danshen (Salvia miltiorrhiza Bunge): a prospective healing sage for cardiovascular diseases. 2017;23(34):5125-35. doi: 10.2174/1381612823666170822101112.

64. Ansari MA, Khan FB, Safdari HA, Almatroudi A, Alzohairy MA, Safdari M, *et al*. Prospective therapeutic potential of Tanshinone IIA: An updated overview. Pharmacological research. 2021;164:105364. doi: 10.1016/j.phrs.2020.105364.

65. Khan FB, Singh P, Jamous YF, Ali SA, Abdullah, Uddin S, *et al*. Multifaceted pharmacological potentials of curcumin, genistein, and tanshinone IIA through proteomic approaches: an in-depth review. Cancers. 2022;15(1):249. doi: 10.3390/cancers15010249.

66. Shi L, An Y, Wang A, Gao Q, Yang YJAJoO. The protective effect of Salvia miltiorrhiza on gentamicin-induced ototoxicity. American Journal of Otolaryngology. 2014;35(2):171-9. doi: 10.1016/j.amjoto.2013.08.022.

67. Fan G-W, Gao X-M, Wang H, Zhu Y, Zhang J, Hu L-M, *et al*. The anti-inflammatory activities of Tanshinone IIA, an active component of TCM, are mediated by estrogen receptor activation and inhibition of iNOS. The Journal of steroid biochemistry and molecular biology. 2009;113(3-5):275-80. doi: 10.1016/j.jsbmb.2009.01.011.

68. Matougui N, Boge L, Groo A-C, Umerska A, Ringstad L, Bysell H, *et al*. Lipid-based nanoformulations for peptide delivery. International Journal of Pharmaceutics. 2016;502(1-2):80-97. doi: 10.1016/j.ijpharm.2016.02.019.

69. Barba A, Dalmoro A, Bochicchio S, De Simone V, Caccavo D, Iannone M, *et al*. Engineering approaches for drug delivery systems production and characterization. International Journal of Pharmaceutics. 2020;581:119267. doi: 10.1016/j.ijpharm.2020.119267.

70. Dabholkar N, Waghule T, Rapalli VK, Gorantla S, Alexander A, Saha RN, *et al*. Lipid shell lipid nanocapsules as smart generation lipid nanocarriers. Journal of Molecular Liquids. 2021;339:117145. doi: 10.1016/j.molliq.2021.117145.

71. Lollo G, Ullio-Gamboa G, Fuentes E, Matha K, Lautram N, Benoit J-PJMS, *et al*. In *vitro* anti-cancer activity and pharmacokinetic evaluation of curcumin-loaded lipid nanocapsules. Materials Science and Engineering. 2018;91:859-67. doi: 10.1016/j.msec.2018.06.014.

72. Turner PV, Brabb T, Pekow C, Vasbinder MAJJotAAfLAS. Administration of substances to laboratory animals: routes of administration and factors to consider. Journal of the American Association for Laboratory Animal Science. 2011;50(5):600-13.

73. Sun J, Xu Z, Hou Y, Yao W, Fan X, Zheng H, *et al*. Hierarchically structured microcapsules for oral delivery of emodin and tanshinone IIA to treat renal fibrosis. International Journal of Pharmaceutics. 2022;616:121490. doi: 10.1016/j.ijpharm.2022.121490.

74. Meng Z, Meng L, Wang K, Li J, Cao X, Wu J, *et al*. Enhanced hepatic targeting, biodistribution and antifibrotic efficacy of tanshinone IIA loaded globin nanoparticles. European Journal of Pharmaceutical Sciences. 2015;73:35-43. doi: 10.1016/j.ejps.2015.03.002.

75. Liu J-R, Chen G-F, Shih H-N, Kuo P-CJP. Enhanced antioxidant bioactivity of Salvia miltiorrhiza (Danshen) products prepared using nanotechnology. Phytomedicine Plus. 2008;15(1-2):23-30. doi: 10.1016/j.phymed.2007.11.012.

الملخص العربى

تأثير التنشينون ٢أ مقابل التنشينون ٢أ المحمل على الناقلات متناهية الصغر على السمية المزمنة المستحدثة من حمض الفوليك على الأنابيب الكلوية الملتفة فى الجرذان

أميرة نعينع[١]، سامية عرفة[١]، مشيرة الهنيدى[١]، أسماء عاشور[٢]، إيمان نبيل[١]

قسم الانسجة وبيولوجيا الخلايا، [١]كلية الطب، [٢]كلية الصيدلة، جامعة الإسكندرية

المقدمة: يرتبط مرض الكلى المزمن بتغييرات دائمة.التنشينون ٢ أ هو منتج طبيعي يمكن أن يكون فعالا للوقاية من مرض الكلى المزمن، ومع ذلك، فإن إنخفاض التوافر البيولوجي الجهازي له يعوق امتصاصه.لذا فإن الصيغة المحملة على الناقلات متناهية الصغرتستطيع التغلب على هذه المشكلة.

الهدف: المقارنة بين التأثير النسيجي للتنشينون ٢أ مقابل التنشينون ٢أ المحمل علي الكبسولات الدهنية المتناهية الصغرعلي السمية المزمنة المستحدثة من حمض الفوليك علي الأنابيب الكلوية الملتفة في الجرذان.

المواد والأساليب: ٤٢ من ذكور الجرذان تم تقسيمها عشوائيا إلى: المجموعة الأولى: مقسمة إلى ٤ مجموعات فرعية تلقت بالترتيب كبسولات ملحية (الضابطة)، بولي ايثلين جلايكول، تنشينون ٢أ و تنشينون ٢أ المحمل علي الكبسولات الدهنية المتناهية الصغر، لمدة ثلاثة أيام متتالية، المجموعة الثانية : تلقت جرعة واحدة من حمض الفوليك، المجموعة الثالثة والرابعة: تلقت بالترتيب تنشينون ٢أ و تنشينون ٢أ المحمل علي الكابسولات الدهنية المتناهية الصغر، مباشرة قبل حقن حمض الفوليك ولمدة يومين متتاليين لاحقا، كل ذلك عن طريق الحقن داخل الصفاق.في اليوم الثامن و العشرون تم ذبح الحيوانات وتم الحصول على عينات الدم لقياس مستويات نيتروجين اليوريا، الكرياتينين ، المالونديالدهيد، ديسميوتاز الفائق الاكسده ،القدرة الإجمالية لمضادات الأكسدة و الانترليوكين ٦ في سيرم الدم. كما تمت معالجة أنسجة الكلى للفحص المجهري الضوئي والالكتروني. أجريت دراسات مورفومترية لقياس نسبة مساحة الكولاجين ومضاد كاسباز ٣ المناعية. و تم تحليل جميع البيانات إحصائيا.

النتائج: أدى تناول حمض الفوليك إلى تغييرات تنكسية واضحة مؤثرة على الأنابيب الملتفة. تم تشويه الخلايا الظهارية مع وجود فجوات و نوي غامقة و مقذوفة و تغيرات في الميتوكوندريا جنبا إلى جنب مع تسلل خلوي و اتساع خلالي مع ترسب الكولاجين، و أدى ايضا إلى زيادة مؤثرة في نيتروجين اليوريا في الدم، الكرياتينين، المالونديالدهيد، الانترليوكين ٦، النسبة المئوية لمنطقة الكولاجين ومضاد كاسباز ٣ المناعية مع انخفاض مؤثر في ديسميوتاز الفائق الاكسده والقدرة الإجمالية لمضادات الأكسدة. كما لوحظ الحفاظ الجزئي للتركيب النسيجي والمعاملات البيوكيميائية في المجموعة الثالثة. وفي الوقت نفسه، أظهرت المجموعة الرابعة نتائج نسيجية وبيوكيميائية مماثلة للمجموعة الضابطة.

الإستنتاج: حافظ التنشينون ٢أ المحمل علي الكبسولات الدهنية المتناهية الصغر على الأنابيب الكلوية من السمية الكلوية المزمنة أكثر من التنشينون ٢أ.